SYNTHESIS AND CHARACTERIZATION OF BINARY AND TERNARY HYDROTALCITES-LIKE COMPOUNDS FOR THE HYDROXYLATION OF PHENOL

by

SINDISIWE FORTUNATE MUTHWA

(B-Tech)

Student No: 20809282

Submitted in fulfilment of the academic requirements for the degree of Master of Applied Science in the Department of Chemistry, Faculty of Applied Sciences

Durban University of Technology

South Africa

Supervisor: Dr. S. Singh

Co-Supervisor: Dr. M.H. Mabaso

August 2017

PREFACE

The experimental work described in this thesis was carried out in the Department of Chemistry, Durban University of Technology and in the School of Chemistry, University of KwaZulu-Natal, Westville Campus, Durban, from January 2015 to September 2016 under the supervision of Dr. S. Singh and co-supervision of Dr. M. H. Mabaso.

These studies represent original work by the author and have not been otherwise submitted in any form for any degree or diploma to any tertiary institution. Where use has been made of the work of others it is appropriately acknowledged in the text.

Student: Miss. S. F Muthwa

Signed:  Date: 23 August 2017

Supervisor: Dr. S. Singh

Signed:  Date: 23 August 2017

Co-supervisor: Dr. M. H. Mabaso

Signed: Date: 23 August 2017

DECLARATION

I, Sindisiwe Fortunate Muthwa, declare that

1. The research reported in this thesis, except where otherwise indicated, is my original research.

2. This thesis has not been submitted for any degree or examination at any other university.

3. This thesis does not contain other person's data, pictures, graphs or other information, unless specifically acknowledged as being sourced from other persons.

4. This thesis does not contain other persons' writing unless specifically acknowledged as being sourced from other researchers. Where other written sources have been quoted, then:
   (a) Their words have been re-written but the general information attributed to them has been referenced
   (b) Where their exact words have been used, then their writing has been placed in italics and inside quotation marks, and referenced.

5. This thesis does not contain text, graphics or tables copied and pasted from the Internet, unless specifically acknowledged and the source being detailed in the thesis and in the References sections.

DEDICATION

This dissertation is dedicated to

- My big brother Mbongeni Muthwa; you have made my dream come true. Thank you for your love, commitment to help at all times, support from the beginning till now. I will forever be grateful and will remain indebted to you for all your efforts towards my education and making sure I have more than I ever wanted in life as a whole.

- My late siblings, my angels Nonhlanhla, Tholakele, Bhekumndeni, Thembeka, Thandazile, Thokozani and Nhlanhla. I will always love you and you'll always have a special place in my heart.

- My older brother Thabani, wife Hlengiwe and my younger brother Sandile and his wife Thembekile.

- My nieces and nephews Nosihle, Nkanyiso, Ozzie, Mkhehla, Nonku, Thando, Njabulo and Snakhokonke (Phuzetsheni).

- Finally, and most important my parents, my late father Mr. Sifiso A. Muthwa and my mother Mrs. Nokuthula P. Muthwa. I love you both so much and thank you for being there for me always, caring for me all the time and your emotional support was very much appreciated.

MUTHWA – MNGUNI, PHUNGAZA, SCUBU ASOSIWA SYAPHEKWA UKUZE SANELE UMFAZI NENDODA, OMHLOPHE OWEHLA NGOLWEMBU.

NGYABONGA KAKHULU

ACKNOWLEDGEMENTS

First and foremost, I would like to thank my God Almighty, Jesus Christ for his love, mercy and kindness at all times. Most of all for the grace to pursue my dream. “Truly, blessing and mercy will be with me all the days of my life, and I will have a place in the house of the Lord all my days”. (Psalms 23 vs 6)

I extend my heart-felt gratitude and appreciation to my supervisors Dr. S. Singh and Dr. M. H. Mabaso for their guidance throughout this research, their support, encouragement and advice which has made this degree possible.

My sincere thanks also to:

- Dr. V. Balaga who mentored and provided insightful comments throughout this study.
- Mrs Mpume Cele for allowing me to use GC in her lab, her words of encouragement, proof-reading and editing this manuscript.
- Chemistry technical staff at DUT, Ms Avy Naicker, Mrs Mavis Xhakaza for helping with TGA analysis, Sandile Majola for assistance with all FT-IR and UV-Vis analysis, Nyanga Cele and Sandile Sthole for ensuring that I had all the chemicals that I needed.
- Myalowenkosi Sabela for assistance with Endnote and Origin.
- Postgraduate students of the Catalysis Research Group, UKZN, Philani Mpungose for assistance with the development of the spreadsheet to analyse data, Drushan Padayachee for XRD analysis, Kershen Naicker for BET analysis and Majid Farahani for calcining my catalysts.
- My friends Kwanele Kunene, Nosipho Cele and Nokubonga Makhanya for constant encouragement and support.
- Lastly, my fiancée Mr. Sbusiso Shange for being my rock throughout this project, support, words of encouragement and for everything.
- National Research Fund and National Skills Fund for financial support.

ABSTRACT

Hydrotalcites (HT) and hydrotalcites-like (HTLc) compounds were synthesized by the co-precipitation method under low supersaturation. The synthesized binary Mg-Al hydrotalcites and ternary Cu/Mg-Al hydrotalcite-like compounds were characterized by various physico-chemical techniques such as inductively coupled plasma-optical emission spectroscopy (ICP-OES), powder X-ray diffraction (XRD), Fourier transform- infrared spectroscopy (FT-IR), ultraviolet-visible (UV-VIS) spectroscopy, thermogravimetric analysis (TGA), scanning electron microscopy (SEM) and BET surface area analysis. Elemental composition generated from ICP-OES data revealed a value of *x* in the region of 0.25 to 0.33 for all the compounds except for the MgAl-11 sample which revealed an *x* value of 0.5 while XRD patterns exhibited characteristic features indicative of an ordered layered material. FT-IR spectra confirmed the presence of characteristic functional groups and interlayer anions. Only Cu^{2+} which has a d^9 configuration was accountable for the bands identified in UV-VIS spectra, whereas both Mg and Al with their d^0 electron configurations showed no absorptive bands in the UV-VIS spectra. During thermal treatment by TGA, typical weight loss of Cu-Mg/Al HTLcs with temperature elevation was observed. The SEM images clearly demonstrated that all the Cu-Mg/Al HTLcs retained their characteristically layered structure morphologies. The BET surface area measurements showed no trend, however the surface area decreased with an increase in the copper concentration in some cases. For the heterogeneous hydroxylation of phenol using H_2O_2 as an oxidant, several reaction parameters such as solvent systems, catalyst amount, temperature, substrate/oxidant ratio, time and solvent volume were investigated. The product stream, monitored by gas chromatography showed that catechol (CAT) and hydroquinone (HQ) were the main products. Non-catalytic (blank) experiments were investigated to determine whether the reactants and the internal standard contributes to the conversion of phenol without the use of a catalyst. All blank reactions showed very low phenol conversions which were less than 1%, whereas the Mg/Al HTs showed low phenol conversions as well. All the Cu-Mg/Al catalysts showed measurable phenol conversion with Cu-Mg/Al-51a giving the highest conversion of 29.9% and a 56 and 44% selectivity towards CAT and HQ, respectively. The Cu-Mg/Al-15b catalyst, which had the lowest copper concentration, showed the lowest phenol conversion of 8.3% with a 55 % CAT selectivity and 45% HQ selectivity. In general, the phenol conversion increased with an increase in copper concentration. This reinforced the

hypothesis that copper was the active centre in this reaction, since no measurable conversion was observed with Mg/Al HTs.

TABLE OF CONTENTS

CHAPTER 2

EXPERIMENTAL METHODS

CHAPTER 3

RESULTS AND DISCUSSION: CATALYST CHARACTERIZATION

CHAPTER 4

RESULTS AND DISCUSSION: CATALYTIC TESTING

ABBREVIATIONS

%	-	percent
°C	-	degrees celsius
Å	-	Angstrom
cm^{-1}	-	per centimeter
cm^3/g	-	cubic centimeter per gram
BET	-	Brunauer-Emmett-Teller
CAT	-	catechol
DTA	-	Differential thermal analysis
EM	-	Electron microscopy
EtOAc	-	Ethyl acetate
EDX	-	Energy dispersive X-ray spectrometry
FID	-	Flame ionization detector
FT-IR	-	Fourier-transform infrared
g	-	gram
GC	-	Gas chromatography
H_2O	-	water
HT	-	hydrotalcite
HTLc	-	hydrotalcite-like compounds
HQ	-	hydroquinone
ICP-OES	-	Inductively coupled plasma- optical emission spectroscopy
JCPDS	-	Joint Committee on Powder Diffraction Standards
LDH	-	layered double hydroxides
MeCN	-	acetonitrile
MeOH	-	methanol
mg/s	-	milligrams per second
mL	-	millilitre
nm	-	nanometre
s	-	second
SEM	-	Scanning electron microscopy
TGA	-	Thermogravimetric analysis
viz.	-	namely
XRD	-	X-Ray diffraction

LIST OF FIGURES

LIST OF TABLES

LIST OF SCHEMES

CHAPTER ONE
GENERAL INTRODUCTION AND LITERATURE SURVEY

1.1 General background

The technology which increases the rate of a chemical reaction is called catalysis. This technical field employs both scientists and engineers. Scientists and engineers use catalyst materials to explore the phenomenon of catalysis [1, 2]. Catalysts are materials which speed up chemical reactions without the catalyst being consumed and are materials which prompt change. In addition, catalysts enhances the rate of chemical equilibrium but they are not changed or consumed in the process [3-5]. A good catalyst must retain high activity and long-term stability. However, its single most important attribute is its selectivity, which reflects its ability to directly change the reactant(s) along one specific pathway [6]. Catalysis can be better understood by considering the general reaction, AB + C → A + BC, as illustrated in Figure 1.1

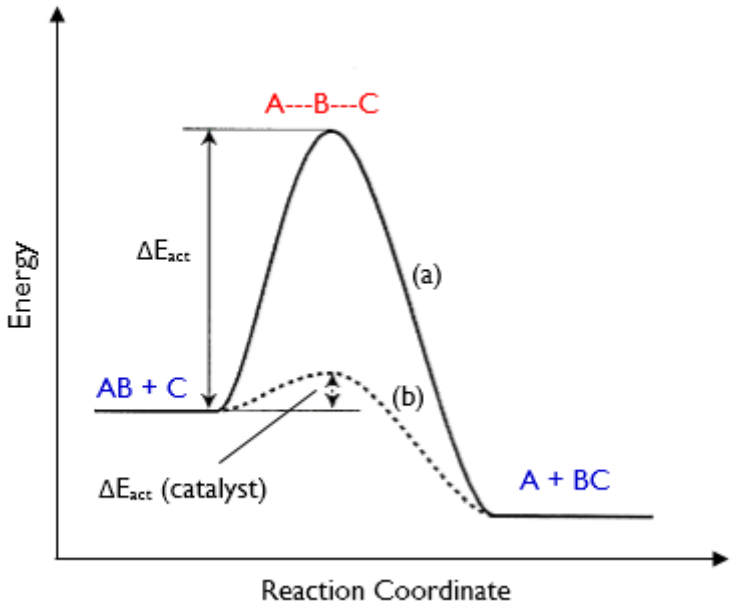

Figure 1.1: Energy profile diagram for (a) uncatalysed and (b) catalysed reaction. (Adapted from [6])

The uncatalysed reaction has to overcome a high energy barrier to form products. The energy required is the activation energy (ΔE_{act}). High activation energies limit the rate of reactions. On addition of a catalyst, the energy barrier is lowered, creating a better chance for the reaction to

take place [3]. The advantages of using catalysts are that milder reaction conditions are attainable with decreased energy consumption and environmentally benign processes are possible. Through the catalytic route, increased reaction rates and increased selectivity are more sustainable. To enhance selectivity of the desired products catalyst can be varied so that less waste is generated, which is extremely necessary, eventually resulting in a lower E factor (the mass ratio of waste and by-products to desired products) and less energy is consumed with higher yields.

Without the use of catalysts, many chemical processes would be commercially non-viable or even impossible. Catalytic chemical synthesis accounts for at least 60 % of chemical products and 90 % of current chemical processes. Starting from the earliest commercial processes, such as the Haber process for ammonia synthesis, catalysts have become a billion dollar global industry, and have an impact on billions more in production. Escalation in the cost of feedstock and energy, demands a continual improvement in the efficiency of catalysts and processes in current use. Choosing the right catalyst can lower the required amount of raw materials, reduce the cost of energy and decrease the quantity of by-product and associated separations cost.

Catalysis can be grouped into three main types, viz. homogeneous catalysis, heterogeneous catalysis and enzyme (biological) catalysis [7-12]. In this study, only heterogeneous catalysts, i.e. hydrotalcites and hydrotalcite-like compounds were considered in the hydroxylation of phenol.

1.2 Hydroxylation of phenol

The hydroxylation of phenol yields two dihydroxybenzenes which are catechol (CAT), also known as pyrocatechol or 1.2-dihydoxybenzene and hydroquinone (HQ), also known as quinol or benzene-1.4-diol [13]. The commercial value and scientific importance is validated by their wide industrial applications. Catechol is used as photographic developer, antioxidant, flavouring agent, in the manufacture of pesticides and is also in the electroplating industry [14]. Hydroquinone is used in pharmaceuticals, drugs and as polymerization inhibitors [15]. The most desirable method for production of dihydroxybenzenes is direct hydroxylation of phenol with hydrogen peroxide (Scheme 1.1). Catechol and hydroquinone are usually formed in the catalytic oxidation of phenol and in some cases further oxidation occurs leading to *para*-benzoquinone being formed [16]. However, catechol's selective conversion of aromatic compounds has always been of great interest to researchers [13, 15]. Catechol and hydroquinone are subsequently attained in parallel processes in the hydroxylation of phenol

using H_2O_2 as an oxidant by the attack of •OH radicals to the aromatic ring. Benzoquinone can be formed by the sequential oxidation of hydroquinone. In addition, a little tar can be formed during the procedure of phenol hydroxylation due to over-oxidation of benzoquinone.

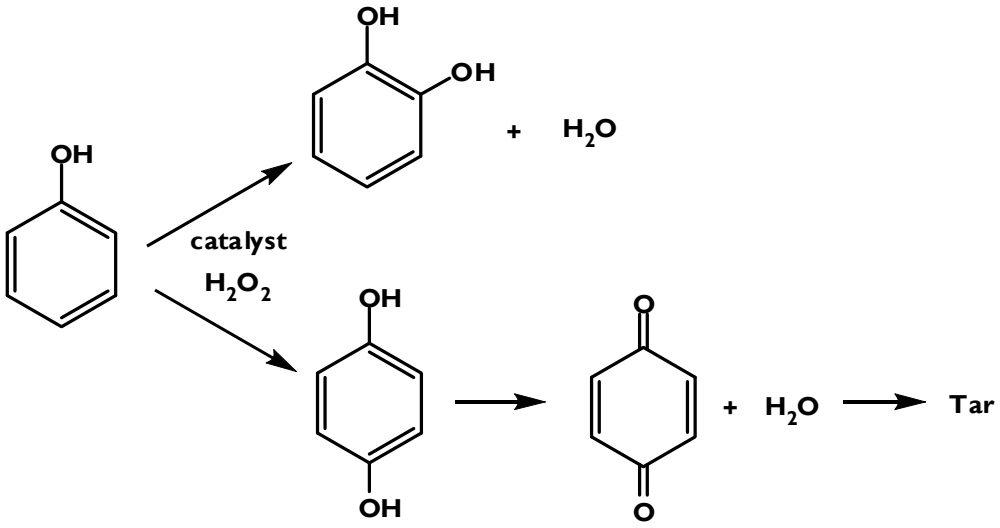

Scheme 1.1 Hydroxylation of phenol

The catalyzed hydroxylation of phenols is carried out using hydrogen peroxide or alkyl hydroperoxides as oxidant [14]. Hydrogen peroxide is a strong oxidizing agent. Although, not as reactive as organic peroxides, it shows good selectivity towards catechol and hydroquinone. Its advantage over the organic oxidants is that it is environment-friendly and leaves only water as the end product. It is also readily available and has been explored as a green oxidant in oxidation reactions [14].

For the hydroxylation of phenol, homogeneous and heterogeneous catalysts have been studied. When homogenous catalysts such as metal complexes, metals ion and mineral acids are used, separation and recovery from the reaction mixture are difficult, as a result this prevents their applications in practical use [17-19]. The use of heterogeneous catalysts such as metal oxides, layered compounds, zeolites and mesoporous materials have has recently been considered for this reaction because of their favourable activities, selectivities and easy separation from the product mixture [20-23]. Therefore, the design of suitable heterogeneous catalysts for hydroxylation reaction has been an important area of research. Also, heterogeneous catalysts are cheap, available, stable and recyclable [18, 20].

1.3 Hydrotalcite and hydrotalcite-like compounds

Clays are found in abundance in nature and are usually formed from the weathering and decomposition of silicate and igneous materials at the surface of the earth [25, 26]. Clays are classified within the phyllosilicates and are layered materials. The layers are based on a two-dimensional stack of inorganic layers. Each layer is composed of either octahedral sheets of hydroxide (LDHs) and metal oxide or tetrahedral sheets of SiO_2, or both [27]. Hydrogen bonding and van der Waals interactions between cations, interlayer anions and water molecules ensure that the layered organization is maintained between subsequent sheets. Clays are classified into two broad groups, namely, cationic clays and anionic clays. Hydrotalcite and hydrotalcite-like compounds belong to the anionic group of clays. The structure of the anionic clays is based on brucite, $Mg(OH)_2$ instead of silicate even though anionic clays are classified as phyllosilicate clay materials. The Mg^{2+} cation is surrounded octahedrally by the hydroxyl groups forming an infinite sheet or layer (Figure 1.2 Cation substitution or replacement is also possible giving rise to a wide variety of isomorphous materials. When cations with a higher valency replaces the cation within the brucite-like sheet, the brucite-like sheets allow an overall positive charge in which counter balance is provided by extra-framework interlayer anions [25-28].

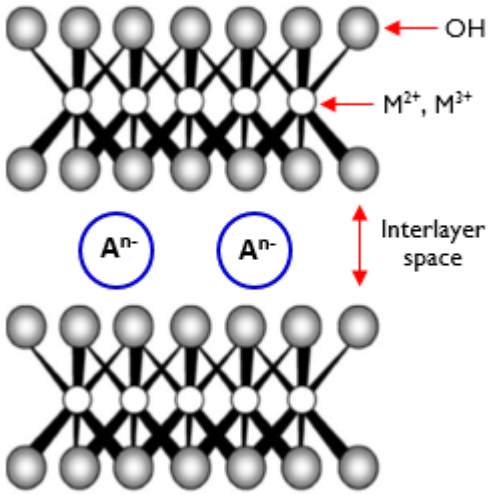

Figure 1.2: Hydrotalcite structure showing the brucite-like layers and interlayer anions [29].

Hydrotalcites (HT) are naturally occurring hydroxycarbonate of magnesium and aluminum, discovered in Sweden in 1842 [29]. Hydrotalcites-like compound (HTlc) or layered double hydroxides (LDH) are the terms adopted to define synthetic compounds based on the

hydrotalcites structure. Manasse [30] proposed the first structural formula for hydrotalcites in 1915 and he acknowledged that carbonate ions are an important part of the structure of these compounds [30]. Literature concerning synthetic hydrotalcites was published by Das *et al*. [31] and Feitknecht [32, 33]. He suggested that the hydrotalcites-like structure constituted of a layer of hydroxide of one cation intercalated with a layer of hydroxide of the second cation. Allman [34] and Taylor [35] performed X-ray studies on these compounds and concluded that the cations are located in the same layer and only the water molecules and anions are located in the interlayer.

Interest in these types of compounds has grown significantly and is reflected by the extensive amount of open literature, both papers and review articles in the fields of catalyst characterization, preparation methods and applications in various types of chemical reactions [36-39] (Figure 1.3).

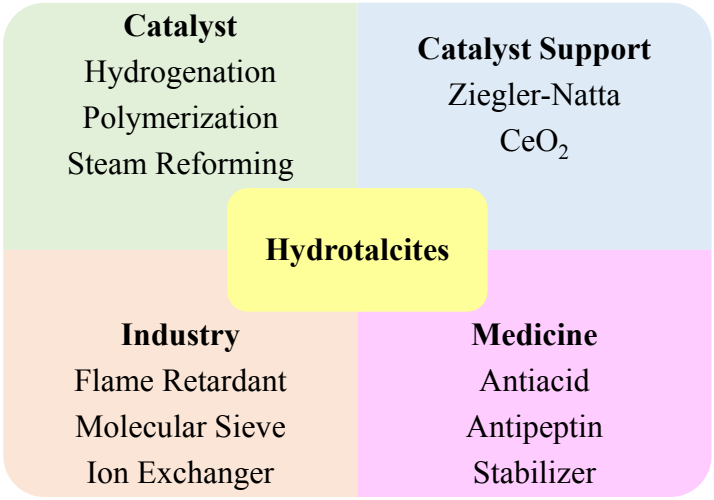

Figure 1.3: Potential applications of hydrotalcite-like compounds [40].

The chemical composition of HT can be represented by, $[M^{II}_{1-x}M^{III}_{x}(OH)_2]^{x+}(A^{n-})_{x/n}.\ mH_2O$ [29], where M^{II} is the divalent metal cation, M^{III}, the trivalent metal cation and A, the interlayer anion. It is essential to start from the structure of brucite, $Mg(OH)_2$ to obtain a better understanding of the structure of HT. The octahedra of Mg^{2+} (6-fold coordinate to OH^-) in brucite share edges to form infinite sheets. These sheets are loaded on top of each other and are held together by hydrogen bonding [41]. With different metal compositions, a series of new types of layered structured compounds can be obtained with similar structure, since the ratio of M^{II} to M^{III} cations can be adjusted within a particular range [42]. To form the HTLc, the main criteria for M^{II} and M^{III} is that their ionic radii must be close to that of Mg^{2+} and Al^{3+},

respectively (Table 1.1) [43]. If the ionic radius of the metal is too large, the octahedral coordination is lost due to opening of one side of the octahedron. This leads to additional coordination with the interlayer water molecule [8]. However, if the ionic radius of a metal cation is too small, it would not fit in the octahedral hole in the brucite-like layer, leading to the collapse of the hydrotalcite structure [43].

Table 1.1: Ionic radii of cations that can be used to synthesize hydrotalcite-like compounds [44].

Divalent cation (M^{II})		**Trivalent cation (M^{III})**	
Metal	**Ionic radii, (Å)**	**Metal**	**Ionic radii, (Å)**
Ca	0.10	**Al**	**0.54**
Fe	0.61	Fe	0.55
Co	0.65	Co	0.55
Ni	0.69	Ni	0.56
Mg	**0.72**	Mn	0.58
Cu	**0.73**	Cr	0.62
Zn	0.74	Ga	0.62
Mn	0.83	Os	0.63
Pd	0.86	Rh	0.67
Cd	0.95	Ru	0.68

1.3.1 The nature of the interlayer anion

The interlayer anion, (A^{n-}) can be an organic or an inorganic compound [45]. The anions and water are randomly positioned in the interlayer region and they are held together by hydrogen bonds [46]. The interlayer anions balance the positively charged brucite-like layers [42, 44]. These anions can be

- the halides; bromide, fluoride and chloride.
- anionic complexes; ferricyanide, ferrocyanide or $[PdCl_4]^{2-}$.
- organic anions; carboxylates and alkyl sulphates.
- oxo-anions; phosphate, sulphate, nitrate, carbonate and bromate.

- oxo and polyoxo-metallates; dichromate, $(Mo_7O_{27})^{6-}$, chromate and $(V_{10}O_{28})^{6-}$.

The hydroxyl groups in the brucite-like sheet are "tied" to the anions (e.g. CO_3^{2-}) directly or via intermediate H_2O through hydrogen bridges, OH-CO_3-HO and/or OH-H_2O-CO_3-HO. The amount of water present in the interlayer spacing can be calculated or determined by thermal gravimetric measurements of weight loss [29].

1.3.2 The value of *x*

To obtain the value of *x* (metal cation ratio), the ratio of the trimetallic cation and the total metal content must be determined, i.e.

$$x = \frac{M^{III}}{M^{II} + M^{III}}$$

The value must be in the range of $0.2 \leq x \leq 0.33$ for the HT or HTLc to form [29]. Hydroxides and other compounds may be formed as impurities if the value of *x* is outside this range [29, 32, 47]. Any ratio above 0.33 results in an electrostatic repulsion between neighboring trivalent metals in the brucite-like layer, whereas the ratio below 0.1 results in the total collapse of the structure [43].

1.3.3 Methods of preparation of hydrotalcite and hydrotalcite-like compounds

There are various methods of preparing these layered compounds. The mechanism for the construction of the structure by the various methods is relatively similar although these methods are quite different. The mechanism is based on precipitation of the metal cations. [43]. A best preparation method does not exist, as a result a preparative method is chosen to suit a specific study. There are several factors that influence the synthesis of HT or HTLc compounds, irrespective of the preparative method (Figure 1.4). The first requirement is to choose the correct ratio of cations. Also, the anion that has to be introduced must be the species present in higher concentration in the solution [45].

1.3.3.1 Precipitation at low supersaturation

This usually occurs at a constant pH in the range 7 to 10 and at temperatures between 60°C and 80°C. Two solutions of known low reagent concentrations are prepared, i.e. the metal solution containing the source of the M^{2+} and M^{3+} for the hydrotalcites-like compounds and a base solution used to maintain the desired pH. These are added drop-wise, i.e. with a low flow to the reaction vessel. This is followed by extensive washing of the precipitate, some ageing and drying at temperatures not greater than 120°C [30, 31]. Compounds produced via this synthetic route are usually more crystalline than those produced using high supersaturation conditions. The product usually consists of a large number of particles that are small in size [48].

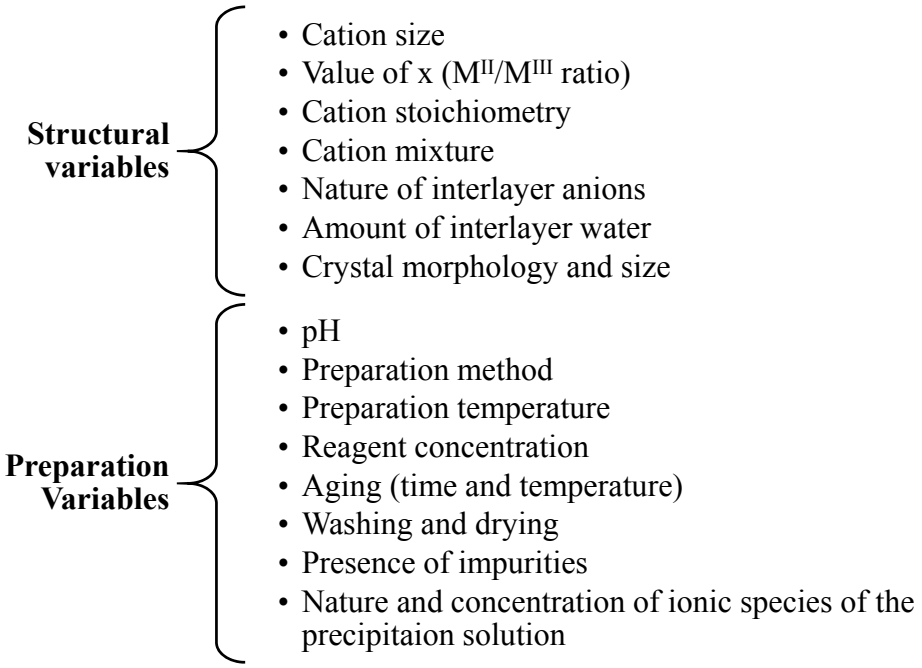

Figure 1.4. Factors influencing the synthesis of HTLc [44].

1.3.3.2 Precipitation at high supersaturation

Preparation of compounds using this method results in materials that are usually less crystalline due to a high number of crystallization nuclei, i.e. the rate of nucleation is higher than the rate of crystal growth. The first patent in the preparation of hydrotalcites-like compounds as catalyst precursors used high supersaturation conditions. $MgAlCO_3$-HT, $NiAlCO_3$-HTLc,

$CoMnAlCO_3$-HTLc, $NiAlCO_3$-HTLc were among the many catalysts synthesized by adding to a solution containing the respective metal salts to a $NaHCO_3$ solution [49].

1.3.3.3 Hydrothermal treatment

In this preparation method, mechanical mixtures of the oxides with water or the hydrothermal treatment of freshly precipitated mixed hydroxides can be used. This is done to improve the crystallinity of an amorphous or poorly crystalline compound or to transform small crystallites into larger ones [31]. High temperature treatments, in this case refer to temperatures higher than 373 K. To achieve this, pressure is essential and synthesis usually takes place in an autoclave [31]. Roy *et al.* were the first to report the preparation of MgAl-HT from a mechanical mixture of MgO and Al_2O_3 [48].

1.3.3.4 Anionic exchange method

HT or HTLc also known as layered double hydroxides (LDH) are a good class of ion exchangers since their lamellar structure which is based on positive layers encompassing anions in the interlayer is highly favourable to anion diffusion [49]. This is useful for the preparation of new compounds represented by

$$[M^{II} - M^{III} - X] + Y \rightarrow [M^{II} - M^{III} - Y] + X$$

Work carried out by Miyata in 1983 reported ion-exchange isotherms of [Mg-Al-X/Y] for a series of monovalent and divalent anions [50]. Thermodynamically, exchange in LDH depends on the interaction of brucite-like sheets and the exchanging anion and, to a smaller extent, the free energy involved in the hydration changes [51]. It was also suggested that exchange is favoured for in-going anions with a high charge density. Kinetically, the rate determining step of the reaction is the diffusion of the in-going anions within the interlayer, provided that the basal spacing of the existing catalyst can accommodate the size of the anion it is to be exchanged with [43]. Synthesis can be relatively simple where an aqueous solution of the LDH precursor is mixed with a large excess of the salt of the anion to be intercalated [43]. The pH of the synthesis is important and this can determine whether or not certain anions are exchanged, e.g. a pH of between 4.5 and 6.0 is required in order to remove either the carbonate or carboxylate anions from a LDH precursor [43].

1.3.3.5 The urea hydrolysis method

HTLc compounds with a uniform crystal size is difficult to synthesize using the conventional constant pH co-precipitation method. The urea homogeneous precipitation method offers a route to control the nucleation rate which controls the particle size distribution of the synthesised HTLc [52, 53]. Urea is a very weak Brønsted-Lowry base and it is very soluble in water. The hydrolysis rate of urea may be controlled by temperature and proceeds in two steps, viz. the formation of ammonium cyanate as the rate determining step (step 1)

$$CO(NH_2)_2 \rightarrow NH_4CON$$

and the fast hydrolysis of the cyanate to ammonium carbonate (step 2) [52, 53]

$$NH_4CON + H_2O \rightarrow (NH_4)_2CO_3$$

The nucleation rate is controlled by changing parameters such as reaction temperature, urea amount, metal salt concentrations and M^{2+}/M^{3+} molar ratio, with temperature is the most important factor [52, 53]. This method has been used for the synthesis of compounds such as NiAl-CO_3, ZnAl-CO_3, MgAl-CO_3, LiAl-CO_3 [54-58].

1.3.3.6 Sol-gel method

The rationale behind sol-gel synthesis is to "dissolve" the compound to a liquid in order to bring it back to a solid state in a controlled manner [52]. The sol-gel method enables mixing at an atomic level which results in the production of a material with a small crystallite size [52, 59]. In addition, it prevents the problem of unhomogeneous particle distribution which is often encountered with the co-precipitation method. Prinetto *et al.* [59] reported on the preparation of Mg/Al and Ni/Al compounds by the sol-gel route performing hydrolysis of alkoxide or acetylacetone precursors with HCl or HNO_3. These were then compared to the to the compounds synthesised by co-precipitation. In all cases, the sol-gel synthesised compounds produced smaller crystallite sizes [59].

1.3.3.7 Microwave-hydrothermal processing

Conventional heating usually involves the use of a furnace or an oil bath, which heats the walls of the reaction vessel where the core of the sample takes much longer to achieve the target temperature [60]. Microwave heating is able to heat the target compounds without heating the

entire furnace or oil bath, saving time and energy. The term "microwave-hydrothermal" processing was coined by Komarneni *et al.* [61] who referred to the reaction taking place in solutions that are heated above 100°C and under the influence of microwave field. For the synthesis of $Mg_3Al(OH)_8NO_3.nH_2O$, aluminium and magnesium nitrate salts were dissolved in de-ionised water and the pH adjusted with NaOH. This mixture was then treated in the microwave cavity for about two hours at 200 psi (≈ 194°C).

1.3.3.8 Post thermal treatment

Thermal treatment is often used for improving the crystallinity of poorly crystallized HTLc [62-64]. The two most commonly used thermal treatment experiments involves heating a closed stainless steel reactor (under pressure) containing an aqueous suspension of HTLc precursor at temperature below the HTLc's decomposition temperature (700°C) [65], while the other involves the heating of the sample in a gold or silver sealed tube under high pressure [62, 63, 65].

Calcination of the hydrotalcite-like materials at temperatures in excess of 400°C yields a mixed oxide structure with a high surface area, typically 100-300 m^2/g [48, 49]. At higher calcination temperatures, the mixed oxide is gradually transformed into two separate phases, a $MgAl_2O_4$, spinel phase and pure MgO [50, 51]. The goal of catalytic research is to improve activity and selectivity by altering the rate constant. Therefore, to obtain a highly active and selective catalyst, calcination up to 500°C which will result in a mixture of MgO and Al_2O_3 for the binary HTLc and CuO, MgO and Al_2O_3 for the ternary HTLc is required. From a catalytic point of view, the synthesis of hydrotalcites with a high surface area, the derived mixed oxides obtained after calcination and their corresponding regenerated hydrotalcites are matters of interest. Subsequently, this should have an influence on the total number as well as the basic strength of the solid and on its catalytic activity. Calcination gives oxides characteristics such as high surface area, basic properties and memory effect which implies that under mild conditions, the original hydrotalcite structure can be reconstructed.

1.3.4 Hydrotalcites and hydrotalcites-like compounds in the catalytic hydroxylation of phenol

Heterogeneous solid catalysts are currently receiving considerable attention because of their unique properties such as easy separation, simple handling, recyclability and low cost [66-71]. These heterogeneous solid catalysts are well suited to replace homogeneous catalysts as they are more environmentally benign and recyclable. HTLc exhibit both Lewis and Brønsted acid sites on the edges of the crystal [65]. The Brønsted acid sites are the external OH^- groups, while the Lewis acid sites are the exposed or the three coordinated M^{3+} ions [66, 69]. Their basic properties make them highly suitable for oxidation reactions. In addition, the catalytic activity of these compounds are related to surface and textural properties, like surface are, particle size, size distributions, and pore shapes [70].

Hydrotalcite-type catalysts have been found to be useful for various types of reactions. They have therefore been well researched and often exploited with environmental and economic concerns being a priority. Uses for these types of catalysts include polymerization of alkene oxides and aldol condensation type reactions. Polyethylene oxide, for example, is used as a water-soluble lubricant for rubber moulds, textile fibres and metal-reforming operations as well as a component in cosmetics and pharmaceuticals [71]. Aldol condensation reactions of aldehydes and ketones have equal industrial importance since they can be condensed to dimeric or higher membered products, e.g. the aldol condensation of acetone to produce mesityl oxide and di-acetone alcohol [72]. These products can be hydrogenated to produce solvents or lubricants or may be used as intermediates in insecticide production.

Lee *et al*. [73] investigated a simple preparation method for Mg–Al hydrotalcites as base catalysts, their memory effect and base catalytic properties. They employed glucose isomerization as a model reaction to explore the catalytic base properties of Mg–Al HTs.

A great variety of redox reactions have been catalysed by hydrotalcite-type catalysts. A general feature of the catalysts used is that they contain a substantial amount of transition metals which allows higher stability, activity and longer lifetimes. The catalytic behaviour of these catalysts can be improved by modifying the hydrotalcite-like catalysts through the addition of other elements which do not enter into the brucite like layer or the interlayer, i.e. they are introduced as promoters. A specific example include nitrobenzene reduction over Co-Mn mixed oxides derived from $CoMnAlCO_3$ HT [74].

Several hydrotalcite-type catalysts have been employed in oxidation reactions. Zhu *et al.* [75] investigated copper-containing hydrotalcite-type compounds for the liquid phase

hydroxylation of phenol using hydrogen peroxide as an oxidant. Their results indicate that hydroquinone and catechol formed in ~55:45 ratios [75]. Choudray *et al.* [76] prepared Mg-Al-O-t-Bu HTLc for the epoxidation of olefins using H_2O_2 as an oxidant. The anion incorporated is larger in size than the most common CO_3^{2-} anion and was therefore incorporated into the interlayer by anion exchange.

In various studies, it has been reported that solvents used in the hydroxylation of phenol with hydrogen peroxide as an oxidant affect the catechol/hydroquinone ratio [77-80], e.g. in aqueous acetone, the reaction yields catechol and hydroquinone in approximately equivalent ratio, whereas in aqueous methanol, the hydroxylation occurs with preferential formation of hydroquinone. Potekhin *et al*. [81] presented a review for the hydroxylation of phenol with hydrogen peroxide as an oxidant. The catechol/hydroquinone ratio decreased as the temperature was increased. In addition, at an increased ratio between the initial concentrations of phenol and hydrogen peroxide at elevated temperatures, benzoquinone was also formed and the catalyst was noticeably deactivated as hydrogen peroxide was consumed. The catalyst deactivation was due to the formation of tar which was adsorbed on the surface and in pores of the catalyst. Zapata *et al.* [82] studied the monometallic Co hydrotalcite-like compounds with Co(II) and Co(III) by systematically varying the precipitant agent and the precursors. As the resulting compounds may differ in their thermal behaviour from those predictably synthesized, the thermal study was also presented. The compound was stable until 150°C and was transformed to Co_3O_4. The amorphous Co-complex was the dominant compound and it was stable up to 250 °C. Kishore and Rodrigues [83] reported a systematic study on the selective oxidation of isophorone over M–MgAl ternary hydrotalcites, where M = Cu, Co or Fe, with the aim of clarifying the effect of transition metal cation on their catalytic performance. The redox properties of transition metal ions played an important role in driving the reaction and a reaction mechanism involving predominantly free radicals, were projected.

Kelkar and Schutz [84] presented work that described the new approach to synthesizing hydrotalcite-like materials containing Mg^{2+}, or Ni^{2+}, or Co^{2+}, $A1^{3+}$ and monocarboxylic anions [85, 86]. The synthesis resulted in materials with a unique sheet-like morphology. They described the critical factors and conditions under which the synthesis can be successfully carried out and sheet-like morphology be obtained.

1.4 Motivation of study

The need for the investigation of the catalytic performance of a series of binary hydrotalcites and ternary hydrotalcite-like compounds has become necessary since no research has been reported in literature where these compounds are used for the hydroxylation of phenol using an internal standard to minimise the interferences. Barbosa *et al.* [22] reported the synthesis of magnesium-aluminium hydrotalcite-like compounds with different MgAl atomic ratios and the adsorption of Fe^{3+} tetrasulphonated phthalocyanine on the surface of these hydrotalcites. The hydrotalcites materials were evaluated as heterogeneous catalysts in the oxidation of catechol using hydrogen peroxide as an oxidant. Kannan *et al.* [23] presented a catalytic performance of a series of CuMgAl ternary hydrotalcites with varying the CuMg atomic ratios and keeping the (Cu+Mg)/Al atomic ratios constant for the selective hydroxylation of phenol with hydrogen peroxide as an oxidant in aqueous solution. To understand the influence of the co-cation on the physicochemical properties of transition-metal-containing hydrotalcites, Rives *et al.* [24] studied the effect of the addition of cobalt to CuAl hydrotalcites on the physicochemical properties and catalytic behaviour, in particular, in the hydroxylation of phenol. Although scattered information on MgAl and CuMgAl hydrotalcites is available, a systematic study of the effect of the variation of the binary and ternary atomic ratios in hydrotalcites on their properties for selective catalytic oxidation is still lacking. Therefore, in this study we will report the catalytic performance of a series of binary and ternary hydrotalcites-like compounds with varying the atomic ratios for the hydroxylation of phenol with hydrogen peroxide as an oxidant and the use of a suitable internal standard.

1.5 Project Aim

The aims for this project were

- the synthesis of the HT and HTLcs with different atomic ratios.
- to incorporate copper to form Cu-Mg/Al HTLcs.
- to characterize the synthesized catalysts by ICP-OES, XRD, FT-IR, UV-Visible, SEM-EDX, TG-DTA and BET.
- to investigate the influence and the effect of solvent, reaction time, catalyst amount, temperature, substrate:oxidant ratio and solvent volume to determine the optimum catalytic conditions.

- to conduct catalyst testing under optimum conditions using H_2O_2 as an oxidant.
- to analyse products by gas chromatography with flame ionization detector (GC-FID).

CHAPTER TWO
EXPERIMENTAL

This chapter describes the experimental and analytical set-up used in the study. Catalysts were synthesized by co-precipitation, characterized by several physico-chemical techniques and tested for the liquid phase hydroxylation of phenol under varying conditions.

2.1 Reagents

The reagents and chemicals used in this study are shown in Table 2.1.

Table 2.1: Reagents used in the synthesis of catalysts and the catalytic reaction

Chemicals	Supplier/ Manufacturer
Magnesium nitrate hexahydrate, $Mg(NO_3)_2.6H_2O$, 99% purity	Sigma Aldrich
Aluminium nitrate nonahydrate $Al(NO_3)_3.9H_2O$, ≥ 98% purity	Sigma Aldrich
Copper nitrate trihydrate, $Cu(NO_3)_2.3H_2O$, > 99% purity	Sigma Aldrich
Sodium hydroxide, NaOH	Promark Chemicals
Sodium carbonate (anhydrous), Na_2CO_3	Associated Chemical Enterprises
Liquified Phenol	Sigma Aldrich

2.2 Catalyst preparation

2.2.1 Preparation of hydrotalcite

The hydrotalcite was prepared by co-precipitation. A basic solution containing NaOH (2 M) and Na_2CO_3 (0.125 M) was prepared by dissolving 20.06 g NaOH and 3.31 g Na_2CO_3 in a 250 mL volumetric flask with de-ionized water. A second solution containing the metals was prepared by dissolving 25.64 g $Mg(NO_3)_2.6H_2O$ (0.1 mol) and 37.44 g $Al(NO_3)_3.9H_2O$ (0.1 mol) in a 100 mL volumetric flask with de-ionized H_2O.

These solutions were added drop-wise over a period of 2 hours to a reaction vessel containing 20 mL de-ionized water to facilitate mixing and precipitate formation while maintaining the pH between 8 and 10. The resulting precipitate was stirred at 60°C for 12 hours and filtered. This was followed by extensive washing with de-ionized water until the filtrate was neutral. The product was dried at 110°C overnight in an oven and then ground to fine powder.
The hydrotalcites with different *x* values were prepared by the method described above.

2.2.2 Preparation of Cu hydrotalcite-like compound

A basic solution containing NaOH (2 M) and Na_2CO_3 (0.125 M) was prepared by dissolving 20.83 g NaOH and 3.06 g Na_2CO_3 in a 250 mL volumetric flask and made up in de-ionized water. A second solution containing the metals was prepared by dissolving 5.11 g $Cu(NO_3)_2.3H_2O$ (0.0.021148 mol), 27.17 g $Mg(NO_3)_2.6H_2O$ (0.10574 mol) and 22.47 g $Al(NO_3)_3.9H_2O$ (0.0625 mol) in 100 mL volumetric flask and made up in de-ionized water. These solutions were added drop-wise over a period of 2 hours to a reaction vessel containing 20 mL de-ionized water to facilitate mixing and precipitate formation while maintaining the pH between 8 and 10. The resulting precipitate was stirred at 60°C for 12 hours and filtered. This was followed by extensive washing with de-ionized water until the filtrate was neutral. The product was dried at 110°C overnight in an oven and then ground to fine powder.
Several hydrotalcite-like compounds with different Cu:Mg ratios and different *x* values were prepared by the method described above.

2.3 Catalyst characterization

The synthesized binary and ternary hydrotalcites and hydrotalcite-like compounds were characterized using various techniques including ICP-OES, XRD, FT-IR, TG-DTA, BET surface area measurements and SEM-EDX.

2.3.1 Inductively coupled plasma-optical emission spectrometry

The ICP-OES technique was used to determine the concentration of different metals and their respective ratios at which they are present in the synthesized catalysts. In the preparation of the standards,

accurate masses were used to prepare stock solutions of Cu, Mg and Al (Supplier shown in Table 1.1A, Appendix 1A) in 500 mL volumetric flasks to make up 100 ppm stock solutions. The actual parameters are shown in Table 2.1A, Appendix 2A. Multi-element standard solutions containing Cu^{2+}, Mg^{2+} and Al^{3+} cations were prepared from the 100 ppm stock solutions of each element and calibration standard concentrations of 5, 10, 15, 20 and 25 ppm for each element were prepared by diluting appropriate volume of 100 ppm into 100 mL volumetric flasks (Table 2.2A, Appendix 2A).

In the preparation of the sample, an accurately weighed mass (Table 2.3A, Appendix 2A) was dissolved in 5 mL of concentrated HCl. The solution was then heated on a hot plate to achieve dissolve the solid catalyst. The solution was cooled to room temperature and filtered by gravity into a 100 mL volumetric flask. The sample was then diluted to volume with deionized water. Both the standards and the sample were then analyzed by a SHIMADZU, ICPE-9000 Plasma Atomic Emission Spectrometer.

2.3.2 X-ray diffraction

X-ray diffraction **(**XRD) analysis provides additional information beyond basic identification. Other information obtained can include the degree of crystallinity of the mineral. To obtain XRD "fingerprints" for the synthesised HT and HTLcs, the catalysts were first ground into fine powder. The material was then scanned within a 2 theta range of 5° to 70° at 0.5 degrees per minute using a Bruker D8 Advance instrument equipped with a Bruker Vantec detector. Runs were carried out using a Cu Kα radiation source, $\lambda = 1.5406$ nm at a voltage and current of 40 kV and 40 mA, respectively.

2.3.3 Fourier Transform infra-red spectroscopy

Fourier Transform infra-red Spectroscopy (FT-IR) is a vibrational spectroscopic technique which provides important information, such as the presence of different anions in the interlayer space between the brucite-like sheets, the orientation of the anion and the different types of bonds that the anions form [87].

A Varian 500 FT-IR Scimitar Series was used to obtain spectra of the synthesized compounds using the KBr disc method. About 0.1 g of dry KBr and approximately 0.001 g of the sample

were ground to a fine powder using a pestle and mortar. The sample was then added to a die, which was subsequently subjected to vacuum (~10 min) to remove the air from the disk.
The disk thus formed was loaded onto a sample holder. The IR spectra were recorded in the range of 380 to 4000 cm^{-1} and analysed using Varian Resolution 4.0 Software.

2.3.4 Thermal gravimetric-differential thermogravimetric analysis

Thermal gravimetric-differential thermogravimetric analysis (TG-DTA) is a method of thermal analysis in which changes in chemical and physical properties of the catalysts are measured as a function of increasing temperature [88, 89]. For hydrotalcites, the change in physical form (weight loss) is dependent on many factors, the most significant are the type of the anion and the ratio of M^{II}/M^{III} [89, 90].
For TG-DTA analysis, compound was placed on a crucible pan in a Metler Toledo TGA/DSC instrument under nitrogen flowing at a rate of 100 mL/min. The heating rate was 10°C/min from 25 to 1000°C.

2.3.5 BET surface area and pore volume measurements

The BET technique uses a gas adsorption method to determine the surface area and pore size distribution of porous and finely divided materials. Nitrogen is the most commonly used gas in BET surface area measurements [91].
The BET surface area and pore volume studies were carried out by degassing the catalysts under N_2 flow overnight at 200°C using a Micrometrics Flow Prep 060. The degassed samples were analyzed in a Micrometrics ASAP 2020 multi-point BET surface area analyzer.

2.3.6 UV-Visible spectroscopy

UV-Visible spectroscopy was conducted on the synthesized catalysts to observe the electronic properties of the metal ions using a Varian CARY CONC UV-Visible spectrophotometer loaded with CARY WinUV Software. Samples were placed in a quartz cuvette, inserted in the instrument and reading recorded over a wavelength range from 180 to 800 nm.

2.3.7 Scanning electron microscopy-energy dispersive X-ray detection

Scanning electron microscopy-energy dispersive X-ray detection (SEM-EDX) reveals information about the surface features of the catalysts, their texture, morphology and metal content [92].

For sample analysis, a strip of double sided carbon tape (Nisshin EM, CO. LTD) was placed onto a SEM stud. Thereafter, each sample was placed onto this stud and carbon coated using a JEOL JEE-4C Vacuum Evaporator. The stud was placed in a LEO 1450 SEM and analysed using SmartSEM Software, Version 5.03.05. For SEM-EDX, a JEOL JSM-6100 Scanning Microscope was used equipped with Bruker Espirit Software, Version 1.9.

2.4 Catalytic testing

The hydroxylation of phenol in aqueous solution was carried out in a 25 mL two-necked pear shaped flask fitted with a condenser and a septum. The oxidant, hydrogen peroxide (30% v/v, 1 mol) was added through the septum to the magnetically stirred solution of the substrate, phenol (2 g, 2 mol) containing the catalyst (0.02 g), internal standard (biphenyl 1 mol) and solvent (10 mL). The reaction temperature was maintained at 60°C. The progress of the reaction was monitored by periodically removing for gas chromatography analysis.

Several solvents such as water, acetonitrile, 1-butanol, methanol, ethyl acetate, acetonitrile:water (9:1) and acetonitrile:ethyl acetate:water (3:3:1) were used in this study. In addition, the influence of reaction temperature and catalyst amount were investigated The reaction was carried out at temperatures of 25, 40, 50, 60, 70, 80, 90 and 100°C with amounts of catalyst varying from 5 to 60 mg.

The product stream was monitored using a SHIMADZU 2014 gas chromatograph equipped with a ZB-WAX PLUS column. Relevant parameters are shown in (Table 1B, Appendix B).

CHAPTER THREE
RESULTS AND DISCUSSION: CATALYST CHARACTERIZATION

3.1 Characterization of catalysts

Catalyst characterization by various techniques was carried out to determine the chemical, physical and textural properties. The different techniques support and complement each other and collectively render the information required to establish the properties of the catalytic material as well as those properties that influence the catalytic activity. Additionally, characterization of the synthesized catalysts revealed the changes to the catalyst induced by its use in the reaction. Every effort has been made to establish the link between the structure of the material and its associated contribution to activity/reactivity.

3.1.1 Inductively coupled plasma-optical emission spectroscopy

The presence of the three metals, viz. Mg, Cu and Al were quantitatively determined by ICP-OES and the results are shown in Table 3.1 and 3.2. The chemical formula of the catalysts, calculated from metal concentrations derived from ICP-OES clearly resemble the formula of typical hydrotalcite and hydrotalcite-like compounds.

Table 3.1 Elemental composition and chemical formulae of the synthesized HT catalysts

Sample	Mg : Al		*x*	Formula
	Calculated	Measured		
MgAl-31	3.0	2.95	0.25	$Mg_{0.75}Al_{0.25}(OH)_2(CO_3)_{0.13}.0.56H_2O$
MgAl-21	2.0	2.04	0.33	$Mg_{0.67}Al_{0.33}(OH)_2(CO_3)_{0.17}.0.48H_2O$
MgAl-11	1.0	1.31	0.50	$Mg_{0.50}Al_{0.50}(OH)_2(CO_3)_{0.25}.0.31H_2O$

Table 3.2 Elemental composition and chemical formulae of the synthesized HT-like catalysts

Sample	Cu : Mg		(Cu + Mg) : Al		Formula
	Calc.	Meas.	Calc.	Meas.	
CuMgAl-51a		4.85	3.0	3.04	$Cu_{0.63}Mg_{0.13}Al_{0.25}(OH)_2(CO_3)_{0.15}.0.56H_2O$
CuMgAl-51b	5.0	4.83	2.4	2.41	$Cu_{0.58}Mg_{0.12}Al_{0.29}(OH)_2(CO_3)_{0.17}.0.52H_2O$
CuMgAl-51c		5.00	2.0	2.00	$Cu_{0.55}Mg_{0.11}Al_{0.33}(OH)_2(CO_3)_{0.20}.0.48H_2O$
CuMgAl-31a		2.95	3.0	3.00	$Cu_{0.56}Mg_{0.19}Al_{0.25}(OH)_2(CO_3)_{0.15}.0.56H_2O$
CuMgAl-31b	3.0	2.94	2.4	2.45	$Cu_{0.53}Mg_{0.19}Al_{0.29}(OH)_2(CO_3)_{0.17}.0.52H_2O$
CuMgAl-31c		3.00	2.0	1.94	$Cu_{0.48}Mg_{0.16}Al_{0.33}(OH)_2(CO_3)_{0.20}.0.48H_2O$
CuMgAl-11a		0.97	3.0	3.00	$Cu_{0.37}Mg_{0.38}Al_{0.25}(OH)_2(CO_3)_{0.15}.0.56H_2O$
CuMgAl-11b	1.0	1.03	2.4	2.38	$Cu_{0.35}Mg_{0.34}Al_{0.29}(OH)_2(CO_3)_{0.17}.0.52H_2O$
CuMgAl-11c		0.97	2.0	2.03	$Cu_{0.33}Mg_{0.33}Al_{0.33}(OH)_2(CO_3)_{0.20}.0.48H_2O$
CuMgAl-13a		0.34	3.0	3.00	$Cu_{0.19}Mg_{0.59}Al_{0.25}(OH)_2(CO_3)_{0.15}.0.56H_2O$
CuMgAl-13b	0.33	0.34	2.4	2.45	$Cu_{0.19}Mg_{0.53}Al_{0.29}(OH)_2(CO_3)_{0.17}.0.52H_2O$
CuMgAl-13c		0.33	2.0	1.94	$Cu_{0.16}Mg_{0.48}Al_{0.33}(OH)_2(CO_3)_{0.20}.0.48H_2O$
CuMgAl-15a		0.21	3.0	3.04	$Cu_{0.13}Mg_{0.63}Al_{0.25}(OH)_2(CO_3)_{0.15}.0.56H_2O$
CuMgAl-15c	0.20	0.21	2.4	2.41	$Cu_{0.12}Mg_{0.58}Al_{0.29}(OH)_2(CO_3)_{0.17}.0.52H_2O$
CuMgAl-15c		0.20	2.0	2.00	$Cu_{0.11}Mg_{0.55}Al_{0.33}(OH)_2(CO_3)_{0.20}.0.48H_2O$

Calc. – Calculated, Meas. - Measured

3.1.2 X-Ray diffraction

Figure 3.1 shows the diffraction patterns of the hydrotalcites where the equal spacing between planes (003), (006) and (012) indicate the stacking order (JCPDS File No. 41-1428). Additionally, sharp peaks obtained indicates that the catalysts were crystalline. However, for MgAl-11, the diffractogram display a non-smooth baseline and the minor peaks are not that apparent. This could be due to the high *x* stoichiometry causing a collapse of the interlayer and less population by the charge compensation anions. The synthesized HTs have a hexagonal plane at high 2θ values, together with the low intensity shown by a doublet peak due to the (110) and (113) planes. A d-spacing of 11.1 Å indicates the presence of a hydroxide in the material.

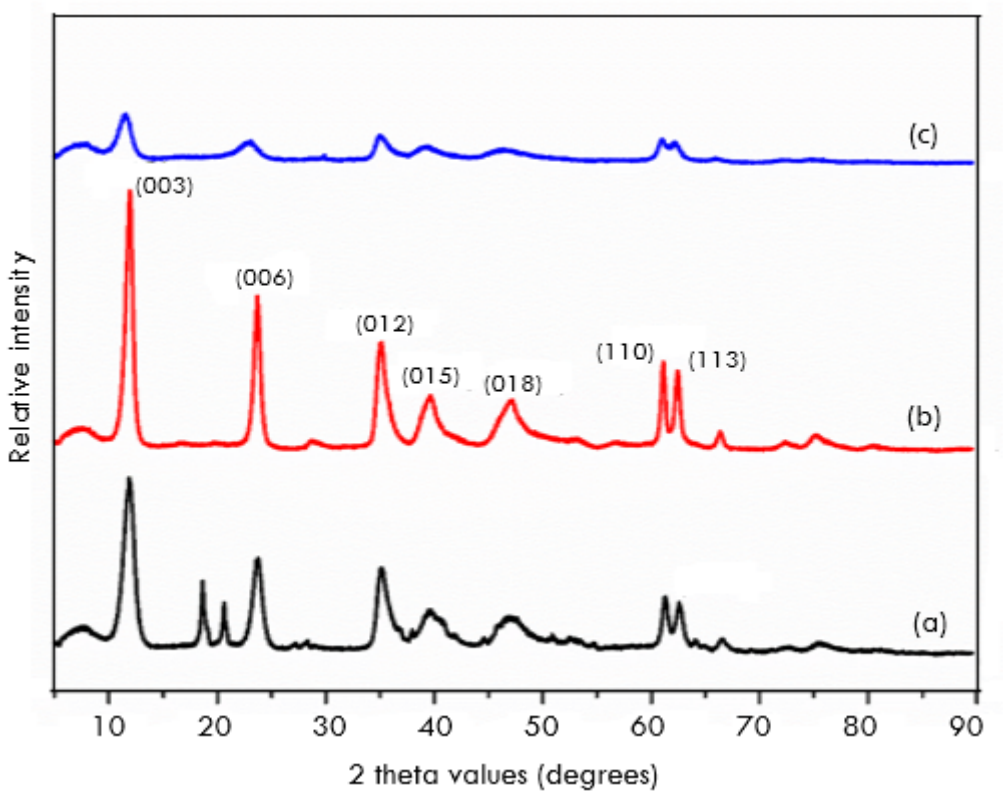

Figure 3.1. Powder X-Ray diffractograms of (a) MgAl-11, (b) MgAl-21 and (c) MgAl-31

All five ternary CuMgAl compounds showed sharp and intense peaks at low diffraction angles with all basal planes corresponding to a layered compound (Figure 3.2). A clear improvement in the order of the layer was noted with low copper content as indicated by both the increase in intensity and sharpness of (110) and (113) reflections observed as a doublet peak around 60º and 62º. At higher copper concentration, the Jahn-Teller distortion leads to poor long-range ordering [23].

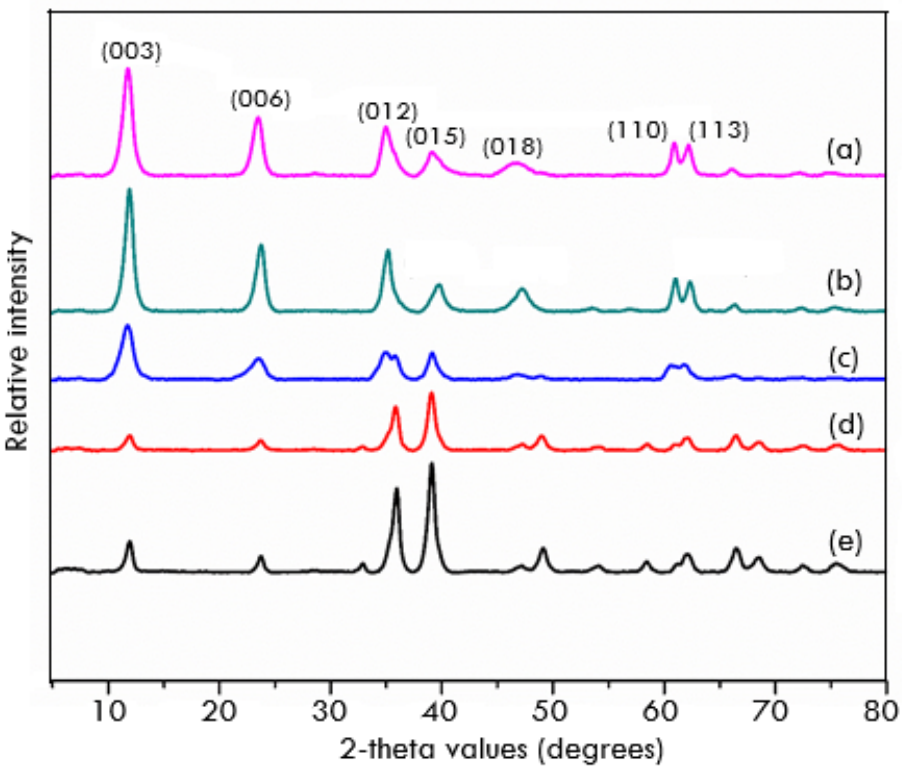

Figure 3.2 Powder X-ray diffractograms of (a) CuMgAl-15b, (b) CuMgAl-13c, (c) CuMgAl-11a, (d) CuMgAl-31a and (e) CuMgAl-51a.

The unit cell of the hydrotalcite displays hexagonal symmetry (Figure 3.3) [32]. Here, *a* represents the average distance between the cations (in the brucite-like structure).

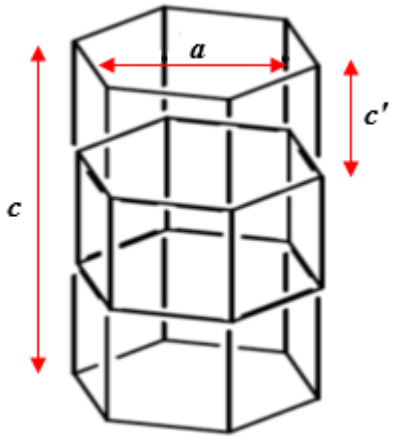

Figure 3.3 Graphic presentation of the unit cell with hexagonal symmetry [32]

To provide additional structural information on the catalysts, unit cell parameters were determined. Here, *a* was calculated using the d-spacing of the first peak in the HT and doublet peak (the 110 plane) and is in agreement with that presented in the literature [93]. The *c* dimension corresponds to thrice the 003 plane d-spacing and is also in agreement with that in literature [23] (Table 3.3 and 3.4).

Table 3.3 Unit cell parameters for the HT samples

Sample	***x***	***a* (Å)**	***c* (Å)**
MgAl-31	0.25	3.04	23.18
MgAl-21	0.33	3.03	22.38
MgAl-11	0.50	3.02	22.39

Table 3.4 Unit cell parameters for the ternary samples

Sample	**Cu: Mg**	**(Cu + Mg):Al**	***x***	***a* (Å)**	***c* (Å)**
CuMgAl-51a	5.0	3.0	0.25	3.06	22.55
CuMgAl-31a	3.0	3.0	0.25	3.09	22.61
CuMgAl-11a	1.0	3.0	0.25	0.08	22.84
CuMgAl-11c	0.33	2.0	0.33	3.08	22.92
CuMgAl-15b	0.20	2.4	0.29	3.07	23.05

3.1.3 Fourier Transform Infra-Red Spectroscopy

Although, infrared (IR) spectroscopy does not provide structural information, it can be used to detect the presence of the carbonate ions and water molecules in the interlayer and the hydroxide groups that make up the brucite-like sheets. The detection of these molecules occurs through the presence of their characteristic vibration and stretching bands. The IR spectra for all three HT catalysts (Figure 3.4) showed similar bands. The presence of water, i.e. the hydration band was observed by the broad band around 3468 cm^{-1} indicating the O-H stretch in the water molecule. A weaker shoulder on doublet peak is observed at around 2361 cm^{-1} which is ascribed to water-carbonate hydrogen bonding within the interlayer region, also

describing the bridging mode of water and carbonate [83, 84]. The shoulder at 1643 cm^{-1} indicate the hydrogen was attributed to the bands around 772 cm^{-1}.

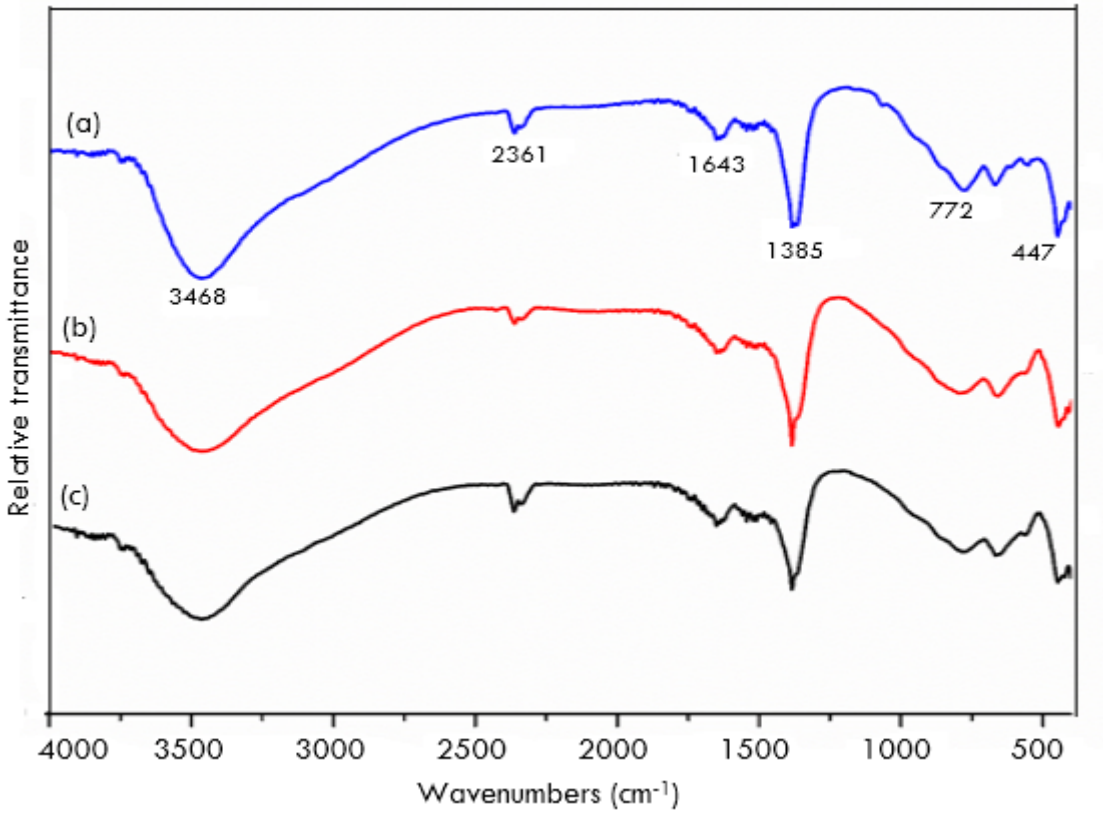

Figure 3.4 FTIR spectra of (a) MgAl-31, (b) MgAl-21 and (c) MgAl-11

The IR spectra of the ternary catalysts are shown in Figure 3.5. According to Panda *et al*. [90], the bands at 550 and 660 cm^{-1} in Figure 3.5 (c), (d) and (e) have a tendency to overlap and hence the appearance as a broader single peak. The sharp band observed at 1002-1050 cm^{-1} (Figure 3.5 (a) and (b)) is due to the v_1 mode of CO_3^{2-} [90]. The appearance of the v_1 mode of CO_3^{2-} is due to a lowering of symmetry of the anion and according to Miyata [91], this is due to the coordination of the carbonate anion within the interlayer. The carbonate anion can exist as a monodendate or bidendate complex [90]. The shoulder at 1643 cm^{-1} is due to the bending mode of interlayer water molecules. A broad band at 3483 cm^{-1} is due to the stretching of the O-H group of the interlayer water molecules [87], the twisting vibrations of physisorbed water, vibrations of hydroxyl groups within the brucite-like layer, characteristic valency vibrations of OH···OH, and/or characteristic stretching vibrations of metal-OH [88]. Weaker doublet peaks are observed at around 2357-2450 cm^{-1} which is ascribed as water-carbonate hydrogen bonding within the interlayer region, also described as the bridging mode of water and carbonate [90].

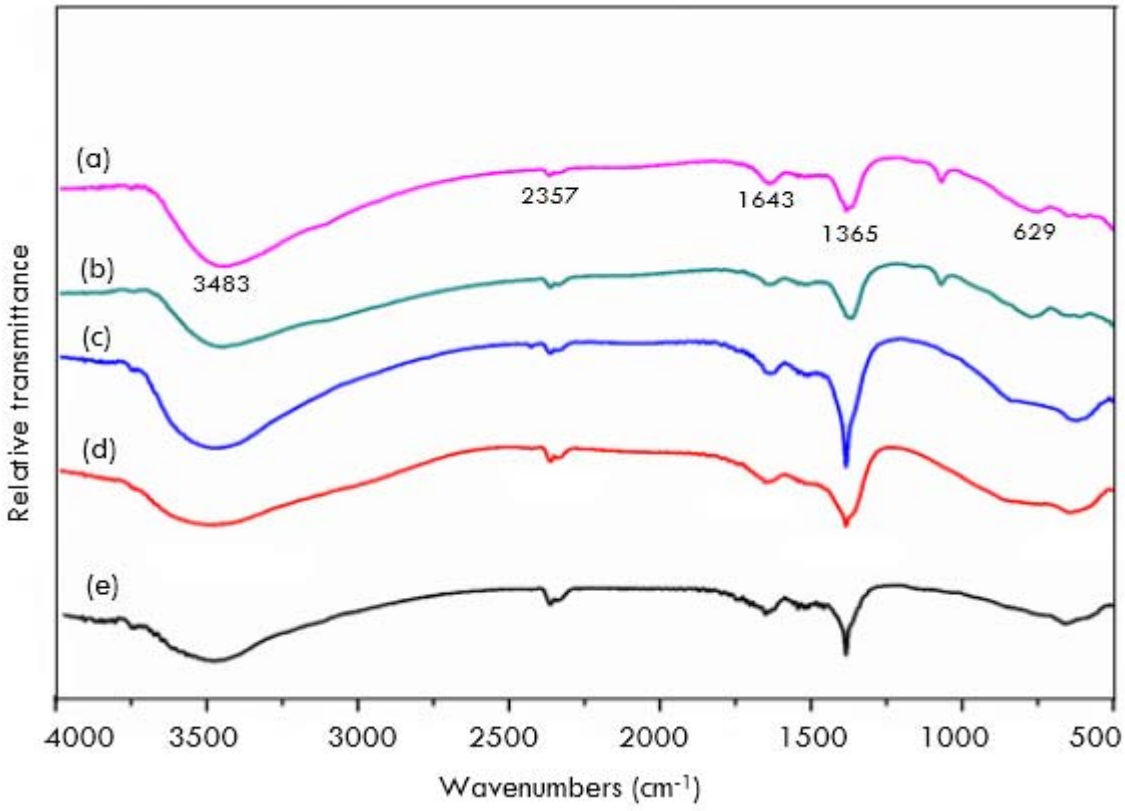

Figure 3.5 FT-IR spectra of (a) CuMgAl-51a, (b) CuMgAl-31a, (c) CuMgAl-11a, (d) CuMgAl-13c and (e) CuMgAl-15b.

3.1.4 Thermal gravimetric-differential thermogravimetric analysis

The thermal stability of the ternary catalysts and its changes in weight with respect to change in temperature was investigated by thermal gravimetric-differential thermogravimetric analysis (TG-DTA) (Figure 3.6 and Appendix 4A). The decomposition behaviour shows that when the catalyst is heated, it releases adsorbed water up to about 100°C. This is followed by the release of interlayer water up to 200°C. Thereafter, the dehydroxylation of the hydroxide layers and decomposition of the interlayer anions between 200 and 350°C [89, 91], the decarbonisation of the carbonate layers at about 600 °C and finally, the formation of mixed phase of MgO and $MgAl_2O_4$ at about 850°C [73].

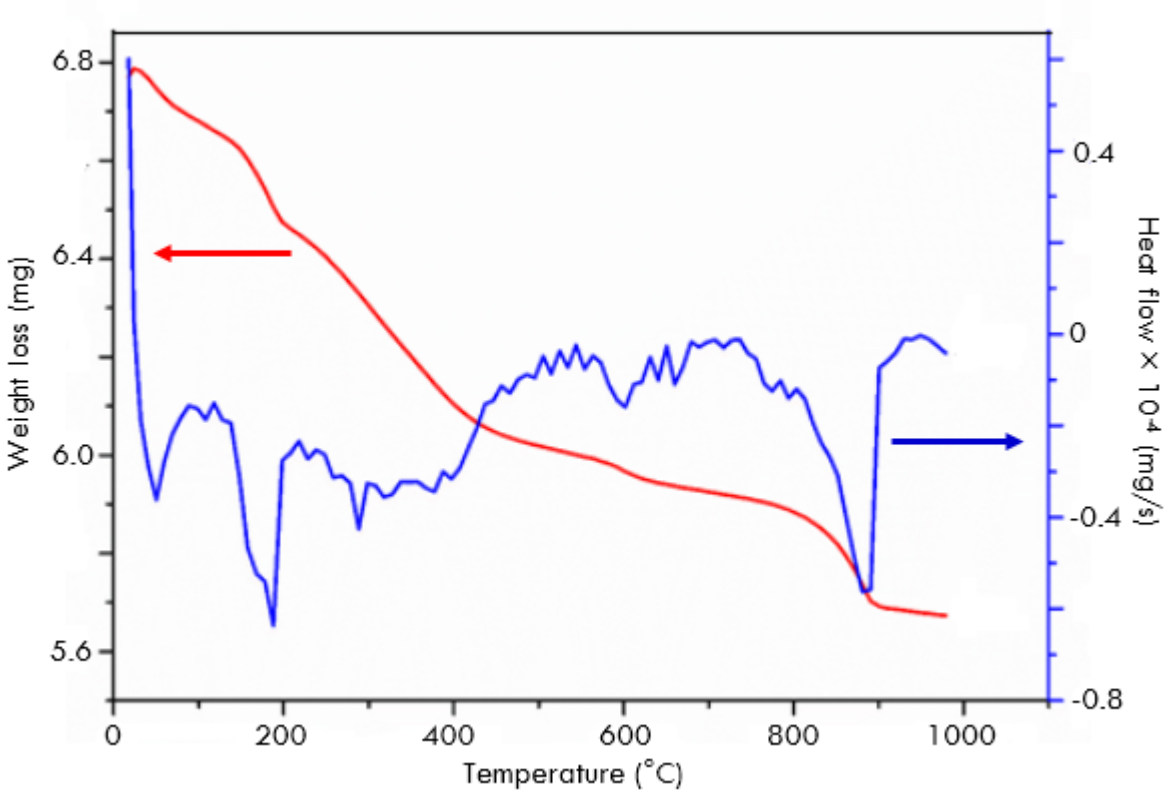

Figure 3.6. TG-DTA of CuMgAl-31a catalyst

3.1.5 BET surface area and pore volume measurements

The results below (Table 3.5) show that the surface area decreases with an increase in the copper concentration.

Table 3.5 Specific surface areas and pore parameters of CuMgAl catalysts.

Sample	Copper content (wt%)	Surface area (m^2/g)	Pore volume (cm^3/g)	Average pore size (Å)
CuMgAl-51a	5	55	0.22	162
CuMgAl-31a	3	60	0.29	189
CuMgAl-11a	1	64	0.32	199
CuMgAl-11c	0.33	96	0.37	154
CuMgAl-15b	0.2	94	0.34	143

Nitrogen adsorption isotherms for the ternary catalysts are shown in Figure 3.7. All the ternary samples showed the type II isotherm according to the IUPAC classification with a relatively small hysteresis loop (Type B) close to a relative pressure of 0.7 to 0.9, indicating a comparable pore construction of largely mesoporous dimensions [72].

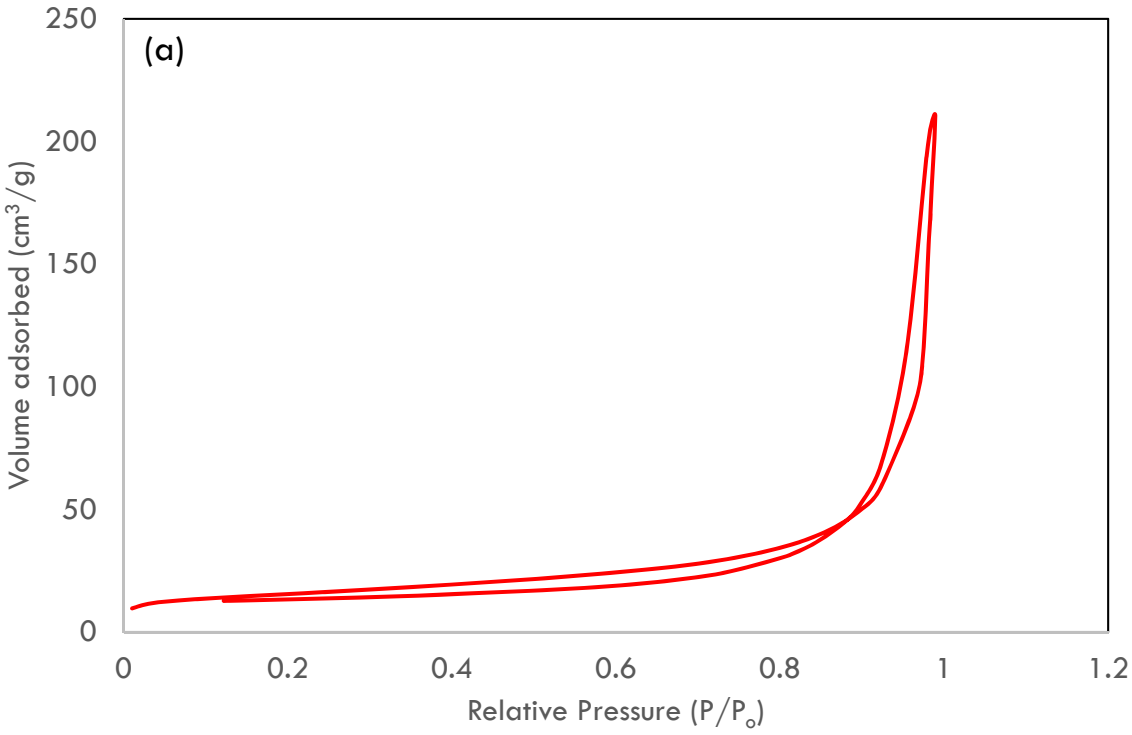

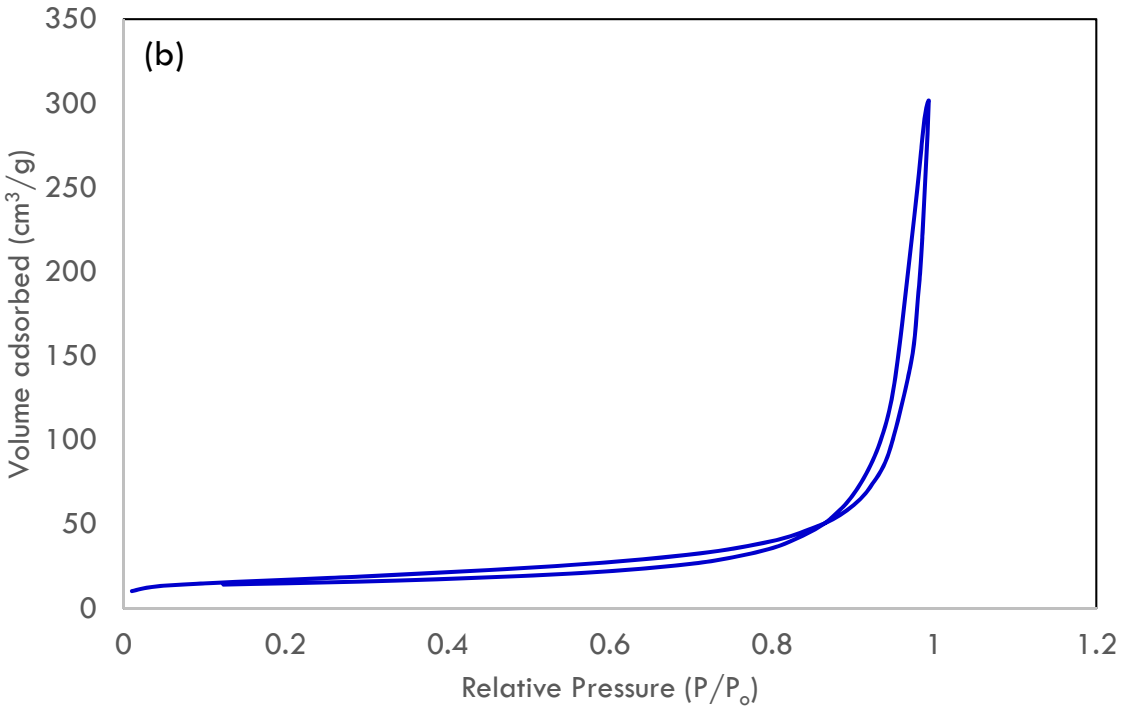

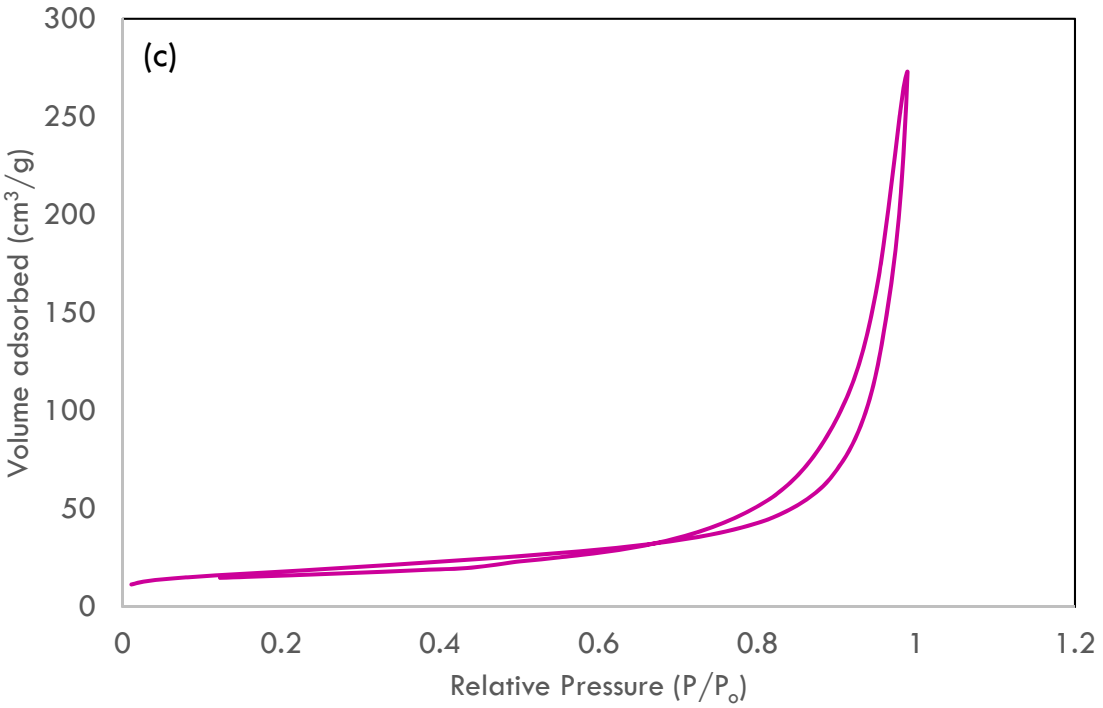
(c)
300
250
200
150
100
50
0
Volume adsorbed (cm3/g)
0
0.2
0.4
0.6
0.8
1
1.2
Relative Pressure (P/Po)

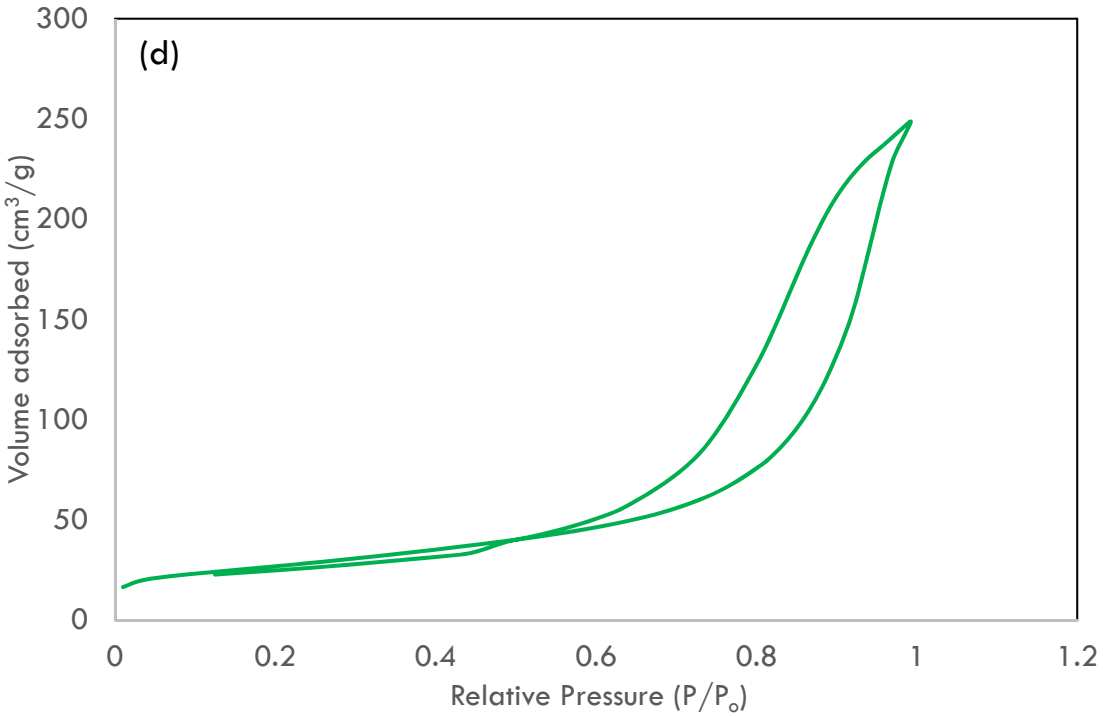
(d)
300
250
200
150
100
50
0
Volume adsorbed (cm3/g)
0
0.2
0.4
0.6
0.8
1
1.2
Relative Pressure (P/Po)

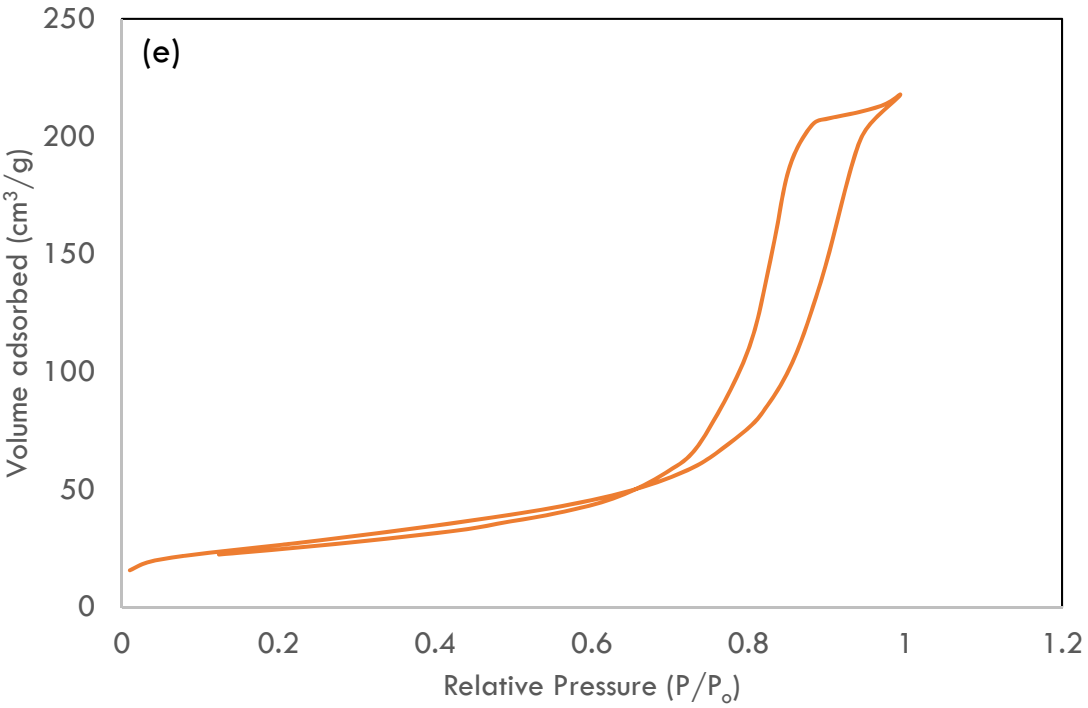

Figure 3.7 Nitrogen adsorption isotherms of (a) CuMgAl-51a, (b) CuMgAl-31a, (c) CuMgAl-11a, (d) CuMgAl-13c and CuMgAl-15b

Furthermore, these results are supported by the pore size distribution of these samples shown below (Figure 3.8). Generally, the distribution of pores is influenced by the crystallite size and packing arrangement of crystallites [71]. A broader distribution of pores was observed for CuMgAl-31a, whereas a relatively narrow distribution of pores was observed for CuMgAl-15b.

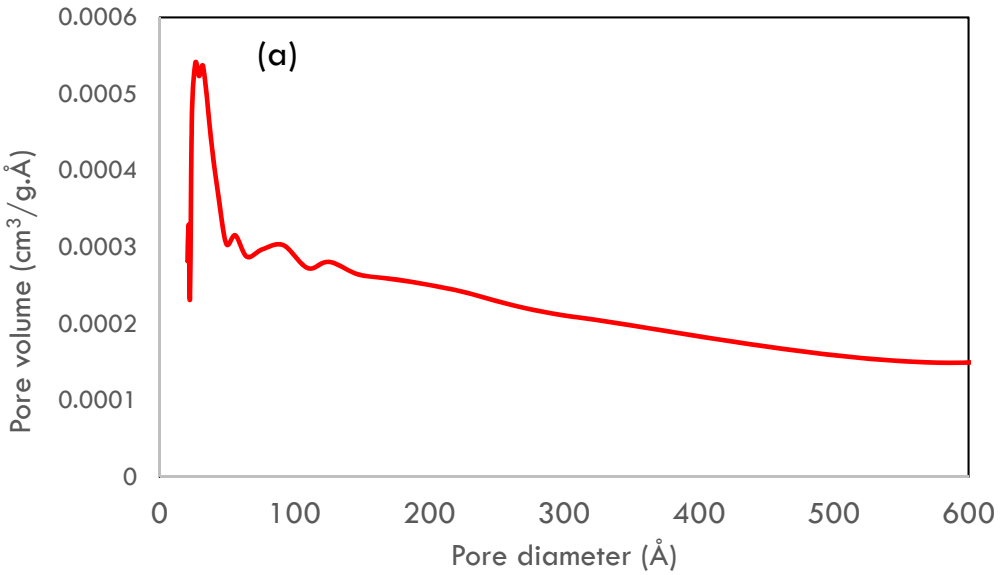
(a)
Pore volume (cm³/g.Å)
0.0006
0.0005
0.0004
0.0003
0.0002
0.0001
0
0
100
200
300
400
500
600
Pore diameter (Å)

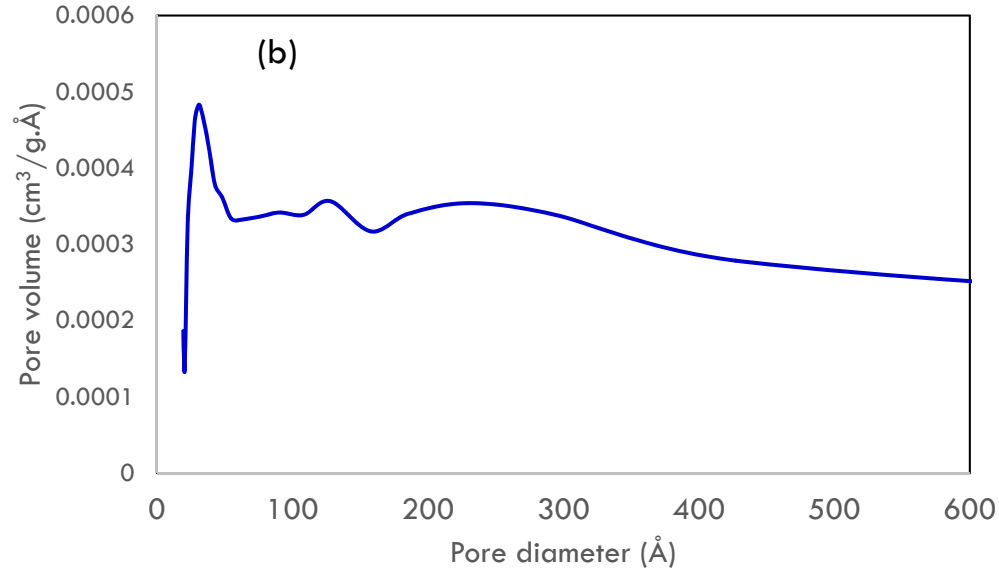
(b)
Pore volume (cm³/g.Å)
0.0006
0.0005
0.0004
0.0003
0.0002
0.0001
0
0
100
200
300
400
500
600
Pore diameter (Å)

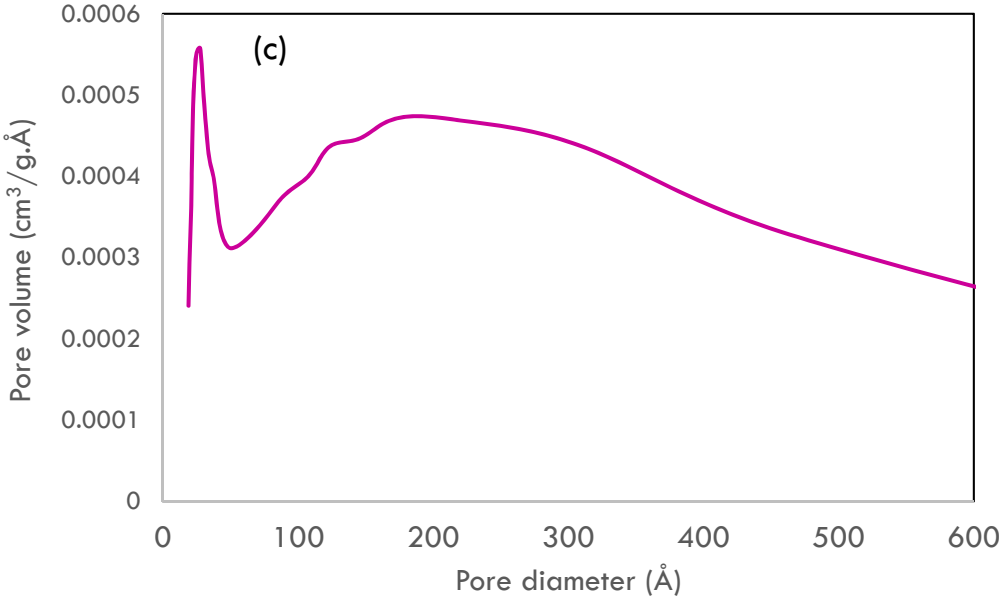
(c)
Pore volume (cm³/g.Å)
0.0006
0.0005
0.0004
0.0003
0.0002
0.0001
0
0
100
200
300
400
500
600
Pore diameter (Å)

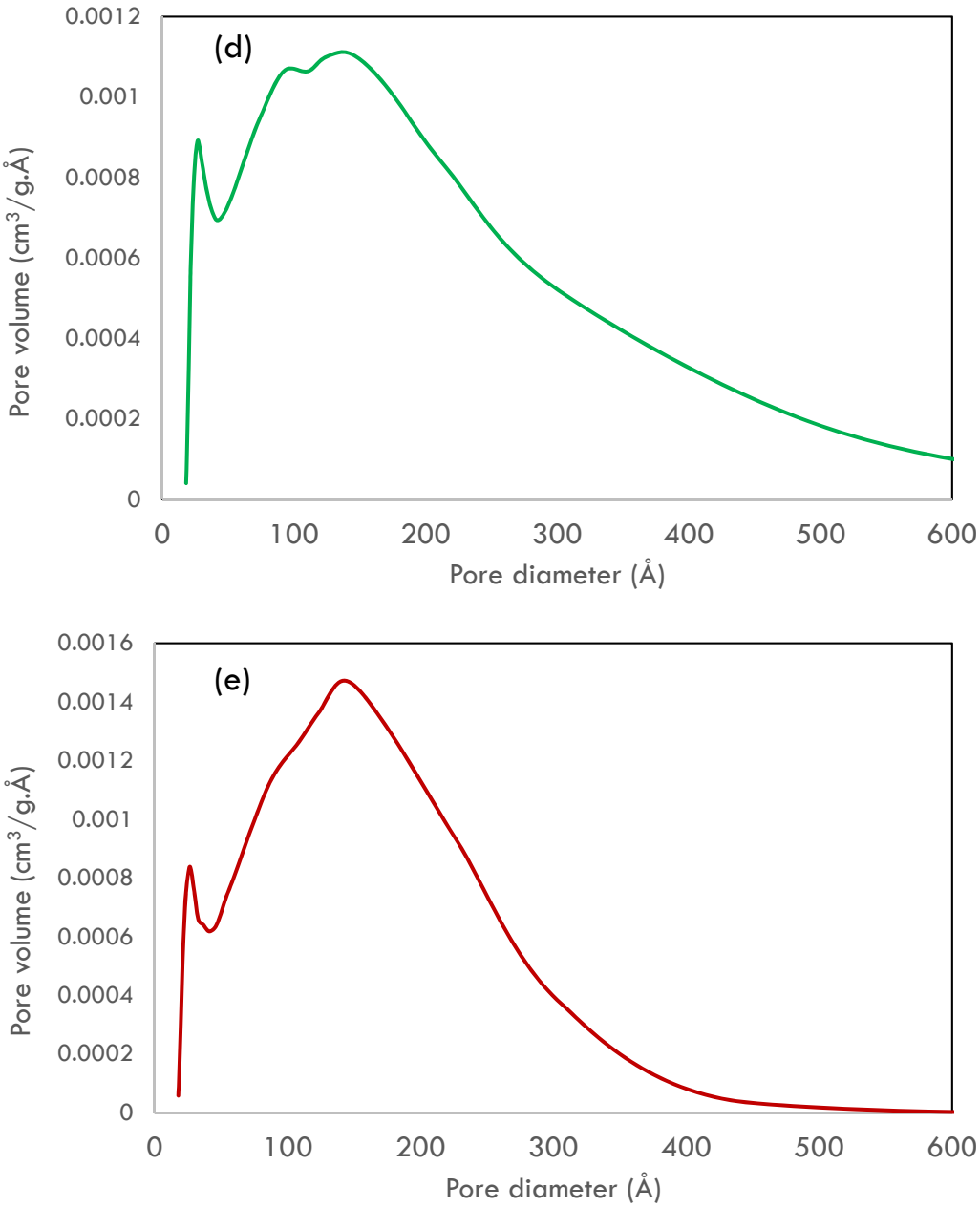

Figure 3.8 Pore size distribution of (a) CuMgAl-51a, (b) CuMgAl-31a, (c) CuMgAl-11a, (d) CuMgAl-13c and CuMgAl-15b

3.1.6 UV-Visible spectroscopy

Due to Mg and Al having d^0 electron configurations, only the Cu^{2+} d^9 electron configuration is responsible for the bands identified in the UV - Visible spectra (Figure 3.9). Similar spectra exhibiting two bands in the region near 255 and 180 nm were showed by all the catalysts. The two bands are generally due to charge-transfer transitions (CT). A decrease in the copper concentration was observed in accordance with a continuous drop in the integral intensities of both bands. The peak around 250 nm could be specifically attributed to an $O^{2-} \rightarrow Cu^{2+}$ charge-transfer transition [91]. Since Cu^{2+} has a d^9 configuration, only one transition is allowed in the visible range.

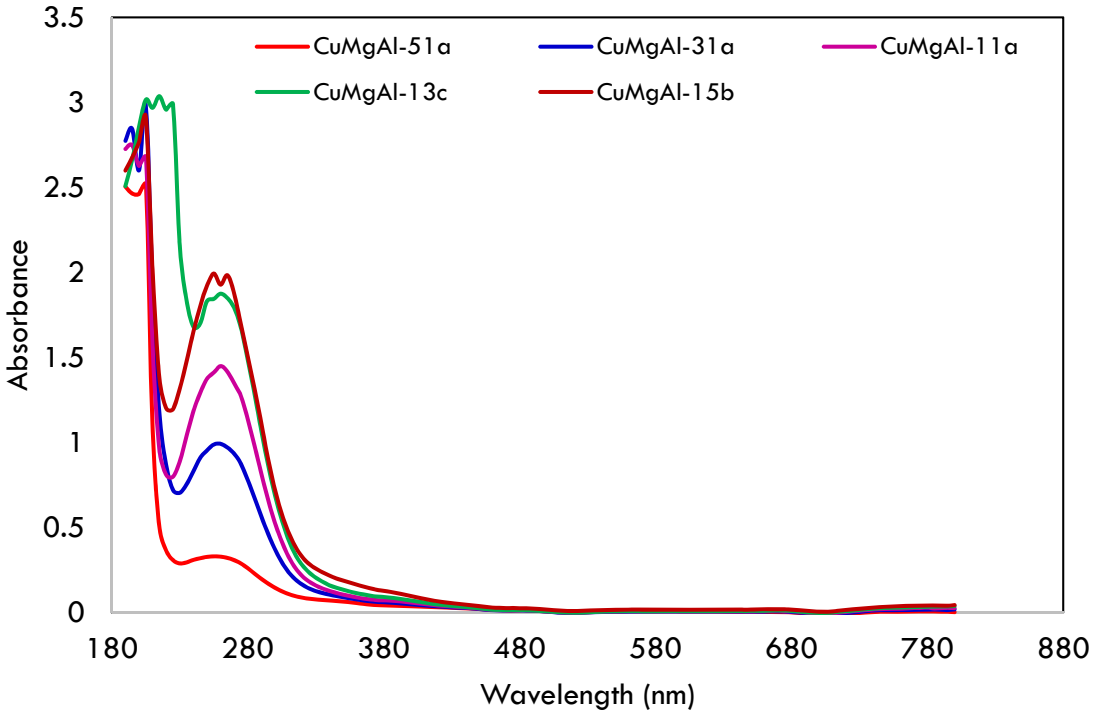

Figure 3.9 UV-Visible spectra of ternary catalysts

3.1.7 Scanning electron microscopy-energy dispersive X-ray studies

The surface morphology of the ternary catalysts and the distribution of the metals, viz.Cu, Mg and Al were investigated by means of scanning electron microscopy (SEM) and energy dispersive X-ray analysis (EDX), respectively. The comparison between the SEM images of all five catalysts (Figure 3.10) show that CuMgAl-51a, CuMgAl-31a, and CuMgAl-11a consist of platelets. Overlapping of such platelets arises, thereby exhibiting a spongy morphology.

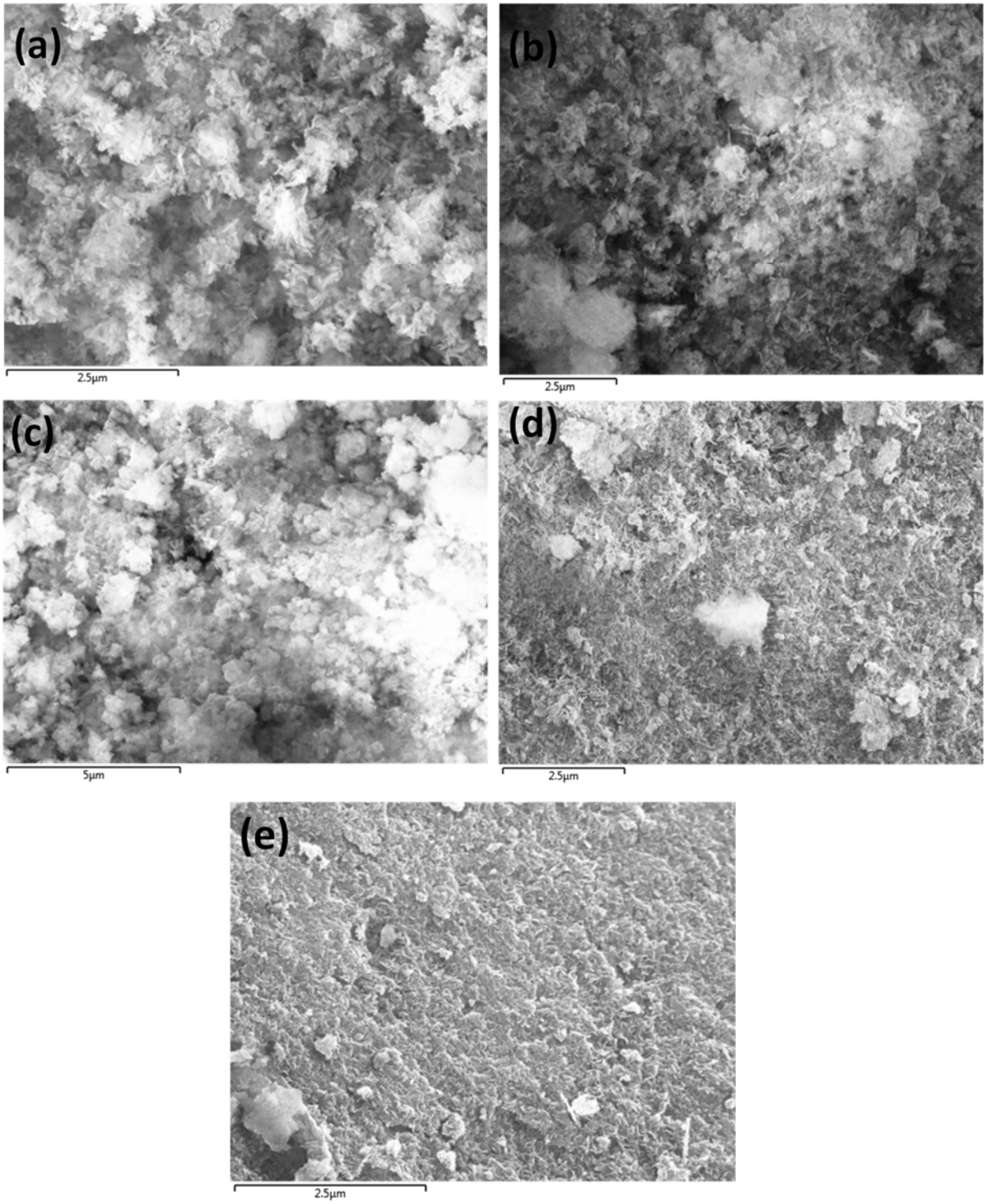

Figure 3.10 SEM images of CuMgAl, (a) 51a, (b) 31a, (c) 11a, (d) 13c and (e) 15b.

EDX images (Figure 3.11) show that Cu is homogeneously distributed in all five catalysts (Cu shown in blue) with no agglomeration, whereas magnesium is randomly distributed.

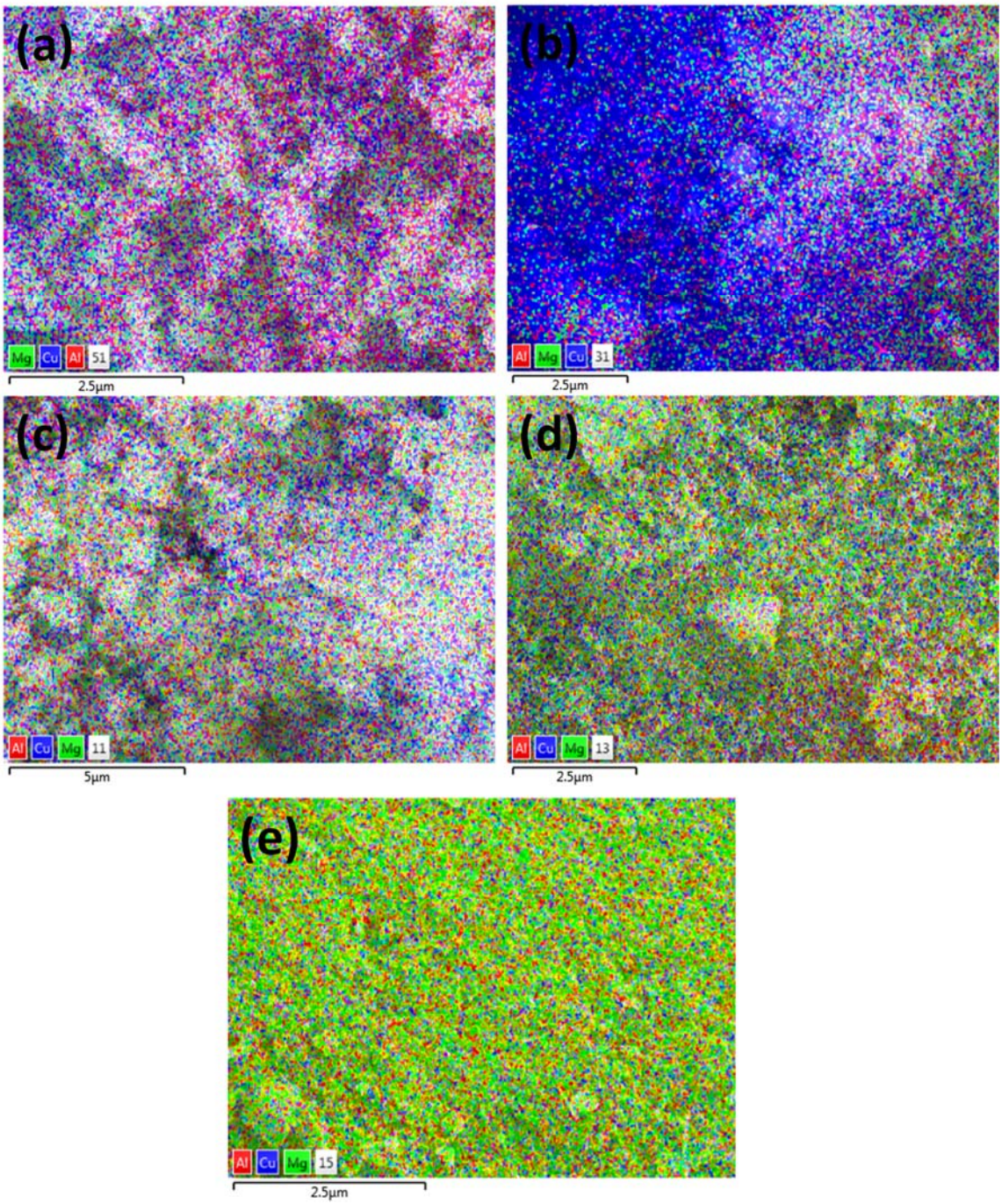

Figure 3.11 SEM-EDX mapping images of CuMgAl, (a) 51a, (b) 31a, (c) 11a, (d) 13c and (e) 15b.

EDX is a localized technique and although the results may vary by a few percent, it is still sufficient to express the elemental constituents of the surface of the catalyst. EDX also gives an idea of the distribution of the elements along the surface. The quantitative results for this study (Table 3.6) suggest that all the elements were incorporated on or near the surface.

Table 3.6. SEM-EDX elemental analysis data

Sample	Elemental %				Atomic %			
	Cu	**Mg**	**Al**	**Total**	**Cu**	**Mg**	**Al**	**Total**
CuMgAl-51a	68.20	10.59	21.21	100	46.77	18.98	34.25	100
CuMgAl-31a	81.30	7.91	10.78	100	63.83	16.24	19.93	100
CuMgAl-11a	51.88	25.09	23.03	100	30.22	38.19	31.59	100
CuMgAl-11c	31.40	25.37	33.23	100	15.54	45.74	38.72	100
CuMgAl-15b	19.01	46.31	34.68	100	8.57	54.59	36.84	100

CHAPTER FOUR
RESULTS AND DISCUSSION: CATALYTIC TESTING

4.1 Blank and optimization studies

Blank experiments were carried out to evaluate the extent of the heterogeneous reaction in terms of the conversion of phenol without the use of a catalyst. For all the blank reactions that were investigated the conversions obtained for all the reactions were very low and hydroquinone was favoured as a major product (Table 4.1). All reactions were done in triplicate and the average within infinitesimal error was reported.

Table 4.1 Blank reaction data

Temperature (°C)	Substrate/Oxidant (mol)	Conversion (%)	Product distribution (%)	
			CAT	HQ
60	2:1	0.3	1	99
	3:1	0.4	23	77
80	2:1	0.3	1	99
	3:1	0.3	11	89

CAT- catechol, HQ- hydroquinone (Reaction conditions: oxidant, H_2O_2; phenol, 1.0 g; biphenyl (internal standard), 1 mol; solvent, acetonitrile:ethylacetate:water (3:3:1), 10 mL; time, 2 h)

4.1.1 Internal standard

The use of internal standards in the hydroxylation reactions has proved to be useful for the calculation of % conversion, % selectivity and this is further applied to the determination of the % yield of the desired products. Initially, *o*-cresol was used as an internal standard in the hydroxylation of phenol reaction, the internal standard was not stable in this catalytic system. Subsequent analysis showed that the peak assigned to *o*-cresol continued decreasing as the reaction proceeded. To understand this, two variations of the general hydroxylation procedure were carried out - one that contained the catalyst and *o*-cresol but no substrate (phenol) and

one that included the catalyst and substrate but no *o*-cresol (i.e. to check whether phenol conversion could take place selectively without interference from the internal standard).

The hydroxylation reaction clearly suggested that o-cresol was reacting under these conditions since after 30 minutes, the peak attributed to o-cresol was no longer present. The chromatogram showed that as the peak for o-cresol decreases, there was a new product peak that was formed before the desired product peaks. Therefore, *o*-cresol was not used as an internal standard.

Further investigations were conducted using biphenyl as the internal standard. The same procedure was followed regarding the variations of the general hydroxylation procedure. The hydroxylation reaction showed that biphenyl was not reacting under the conditions since after 2 hours, the peak attributed to biphenyl was still present and no products were formed which suggested that biphenyl did not oxidise under these conditions but only acts as an internal standard and minimises interferences.

The reaction that included the catalyst and substrate (phenol) had some interference in some cases the phenol peak was not sharp and was broad but with the presence of both the substrate and internal standard the peaks were sharp and intense. Therefore, biphenyl was chosen as the internal standard.

4.1.2 Effect of solvent

Several solvents for the heterogeneous catalytic hydroxylation reactions were investigated (Table 4.2).

Table 4.2 Solvent effect in the hydroxylation of phenol

Solvent	Solubility	Conversion (%)	Product distribution (%)	
			CAT	HQ
Acetonitrile	all reagents dissolved	10.0	81	19
Acetonitrile: water (9:1)	biphenyl partially dissolved	7.4	65	35
Acetonitrile: ethyl acetate: water (3:3:1)	all reagents dissolved	16.6	53	47
Ethyl acetate	all reagents dissolved	4.3	62	38

Reaction conditions: oxidant, H_2O_2; phenol, 1 g; phenol/H_2O_2 molar ratio, 2.0; catalyst mass, 10 mg; internal standard (biphenyl), 1 mol; temperature, 60 ^oC; time, 2 h; solvent, 10 mL.

Acetonitrile and *t*-butanol have comparable boiling points, but significantly different dipole moments. Acetonitrile is an aprotic, medium polarity solvent, whereas *t*-butanol is a protic, medium polarity solvent.

The solvent was chosen based on the following criteria:

- highest conversion rate when all other conditions are kept constant
- form fewer by-products, thus selective towards production of catechol and hydroquinone
- dissolves phenol, biphenyl (internal standard), oxidant and the products
- did not dissolve the catalyst
- do not boil-off at temperatures below 60°C (reaction temperature)
- allowed for product separation

4.1.3 Solvent effect on reaction time

Figure 4.1 shows the variation in the conversion of phenol over some of the solvents investigated at different time intervals at 60°C. From the figure, the maximum conversion was achieved at 60 minutes for both the acetonitrile and acetonitrile/water (9:1 v/v) reactions. Also, a further increase in time did not change the conversion significantly.

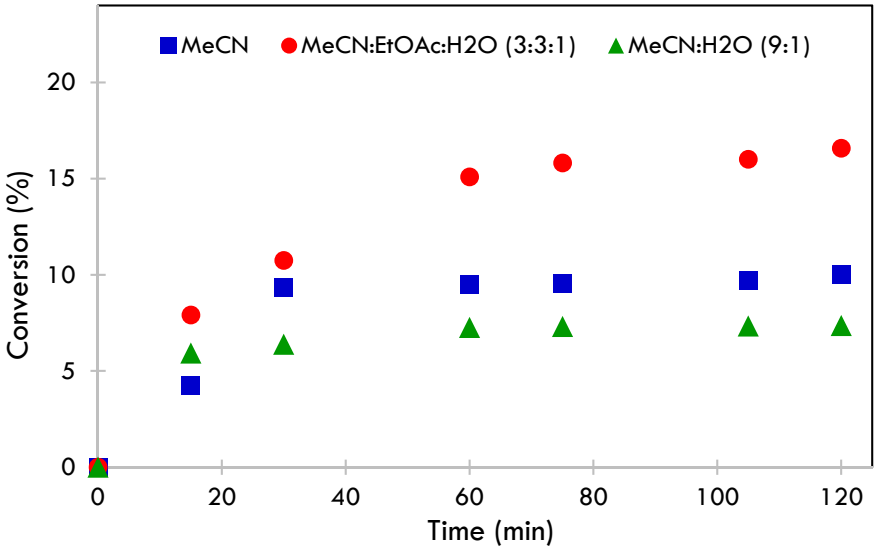

Figure 4.1 Influence of reaction time on the phenol hydroxylation. (oxidant, H_2O_2; phenol, 1 g; phenol/H_2O_2 molar ratio, 2.0; catalyst mass, 10 mg; internal standard (biphenyl), 1 mol; temperature, 60°C; solvent, 10 mL)

However, for the acetonitrile/ethyl acetate/water (3:3:1 v/v) the maximum conversion was achieved at 75 minutes and a further increase in time resulted in a slight change in the conversion. Acetonitrile: ethyl acetate: water (3:3:1) was chosen as the preferred solvent and 120 minutes (2 hours) was chosen as the reaction time.

4.1.4 Influence of catalyst amount

The variation of the catalyst amount (sample loading) for the hydroxylation of phenol was investigated using the CuMgAl-31a catalyst (Figure 4.2). The highest conversion was achieved using 20 mg of the catalyst and the conversion decreased with an increase in catalyst loading. In addition, the preferential formation of catechol was noted at all catalyst loadings.

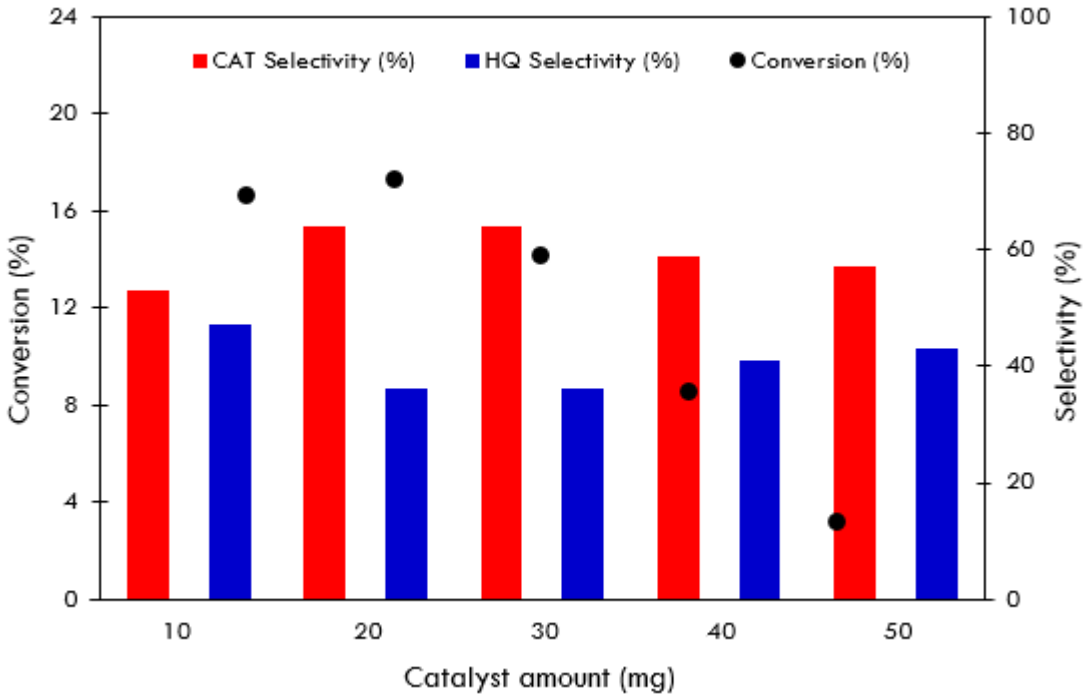

Figure 4.2 Conversion and selectivity as a function of catalyst loading (oxidant, H_2O_2; phenol, 1 g; phenol/H_2O_2 molar ratio, 2.0; solvent, acetonitrile:ethylacetate:water (3:3:1), 10 mL; internal standard (biphenyl), 1 mol; temperature, 60°C; time, 2 h)

4.1.5 Influence of temperature

The variation in the catalytic performance with reaction temperature over the CuMgAl-31a was studied and the results are shown in Table 4.3. A subtle increase in the phenol conversion was noted up to 60°C and further increases in temperature reduced phenol conversion, probably due thermal decomposition of H_2O_2 at higher temperatures. However, the selectivity of catechol and hydroquinone was not influenced by the reaction temperature.

Table 4.3 Influence of reaction temperature on the hydroxylation of phenol over CuMgAl-31a

Temperature (°C)	Conversion (%)	Product distribution (%)			H_2O_2 selectivity (%)
		CAT	HQ	CAT/HQ	
25	0	0	0	0	0
40	5.0	78	22	3.5	8.9
50	13.0	60	40	1.5	25.9
60	17.3	64	36	1.8	34.6
70	15.2	52	48	1.1	30.4
80	10.5	65	35	1.9	20.9
90	5.3	58	42	1.4	10.6

Reaction conditions (oxidant, H_2O_2; phenol, 1 g; phenol/H_2O_2 molar ratio, 2.0; solvent, acetonitrile:ethylacetate:water (3:3:1), 10 mL; catalyst mass, 20 mg; internal standard (biphenyl), 1 mol; time, 2 h). H_2O_2 selectivity calculated on the basis of products formed.

4.1.6 Influence of substrate:oxidant ratio

The effect of the substrate:oxidant molar ratios showed that the conversion increased with the decrease in the ratio (Table 4.4). A continuous increase in the catechol selectivity and subsequent decrease in hydroquinone selectivity was noted with the decrease in the ratio.

Table 4.4 Effect of substrate:oxidant molar ratio over CuMgAl-31a for the hydroxylation of phenol.

Substrate/oxidant mol ratio	Conversion (%)	Product distribution (%)			H_2O_2 selectivity (%)
		CAT	HQ	CAT/HQ	
3:1	10.9	55	45	1.2	32.7
2:1	17.3	63	37	1.8	34.6
1:1	32.1	60	40	1.5	32.1
1:2	37.0	67	33	2.0	18.5
1:3	44.8	68	32	2.1	14.8

Reaction conditions (oxidant, H_2O_2; phenol, 1 g; solvent, acetonitrile:ethylacetate:water (3:3:1), 10 mL; catalyst mass, 20 mg; internal standard (biphenyl), 1 mol; reaction temperature, 60 ^oC; time, 2 h). H_2O_2 selectivity calculated on the basis of products formed.

4.1.7 Influence of solvent volume

The results of the effect of solvent volume is shown in Figure 4.3. The optimum volume of solvent that allowed for maximum conversion was 10 mL.

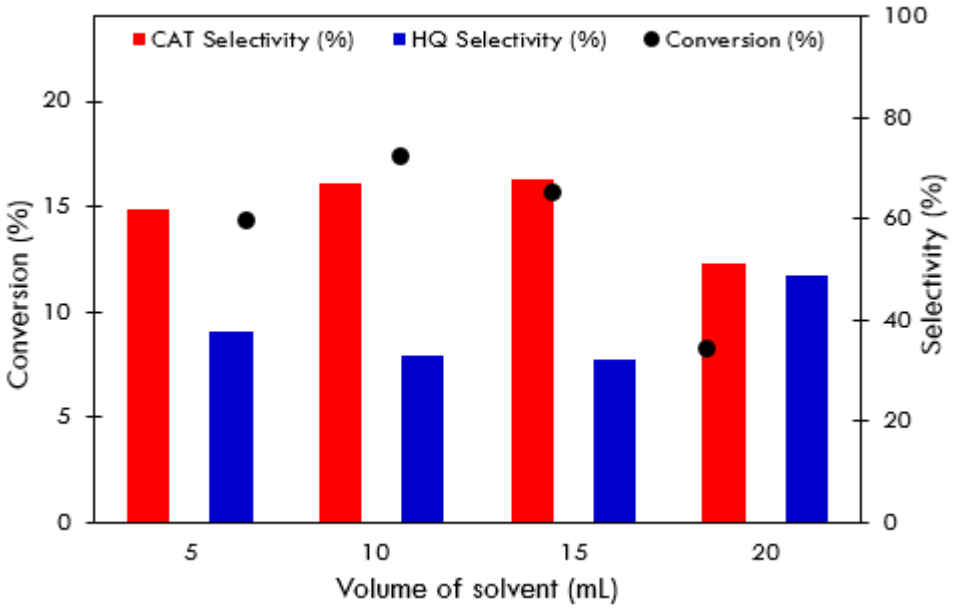

Figure 4.3 Conversion and selectivity as a function of solvent volume (oxidant, H_2O_2; phenol, 1 g; phenol/H_2O_2 molar ratio, 2.0; solvent, acetonitrile:ethylacetate:water (3:3:1); catalyst mass, 20 mg; internal standard (biphenyl), 1 mol; reaction temperature, 60°C; time, 2 h)

4.2 Catalytic testing of the hydrotalcites and hydrotalcite-like compounds

The HTs did not show measurable conversion under investigated conditions (Table 6.2A, 6.3A, Appendix 6A). This cocurs with the study by Zhu *et al* [75] who also observed minimal activity in the phenol hydroxylation using binary MgAl, ZnAl, CoAl and NiAl catalysts.
The ternary Cu catalysts all gave measurable conversions with catechol and hydroquinone formed as major products (Table 4.5 and Table 6.4A, Appendix 6A).

Table 4.5. Hydroxylation of phenol activity over CuMgAl catalysts

Catalyst	Conversion (%)	Product distribution (%)		
		CAT	HQ	CAT/HQ
CuMgAl-51a	29.9	56	44	1.3
CuMgAl-31a	17.3	67	33	2.0
CuMgAl-11a	14.3	61	39	1.6
CuMgAl-13c	10.7	59	41	1.4
CuMgAl-15b	8.3	55	45	1.2

Reaction conditions: oxidant, H_2O_2; phenol, 1 g; phenol/H_2O_2 molar ratio, 2.0; solvent, acetonitrile:ethylacetate:water (3:3:1), 10 mL; catalyst mass, 20 mg; internal standard (biphenyl), 1 mol; reaction temperature, 60°C; time, 2 h.

Among the catalysts studied, CuMgAl-31a showed a product distribution with 67 and 33% selectivity towards catechol and hydroquinone, respectively. Additionally, the CAT/HQ product distribution indicated a ratio of 2.0 which was higher than that of all five samples that were investigated. Furthermore, CuMgAl-15b gave the lowest CAT/HQ ratio of 1.2 and a product distribution of 55 and 45% selectivity towards CAT and HQ, respectively (Figure 4.4).

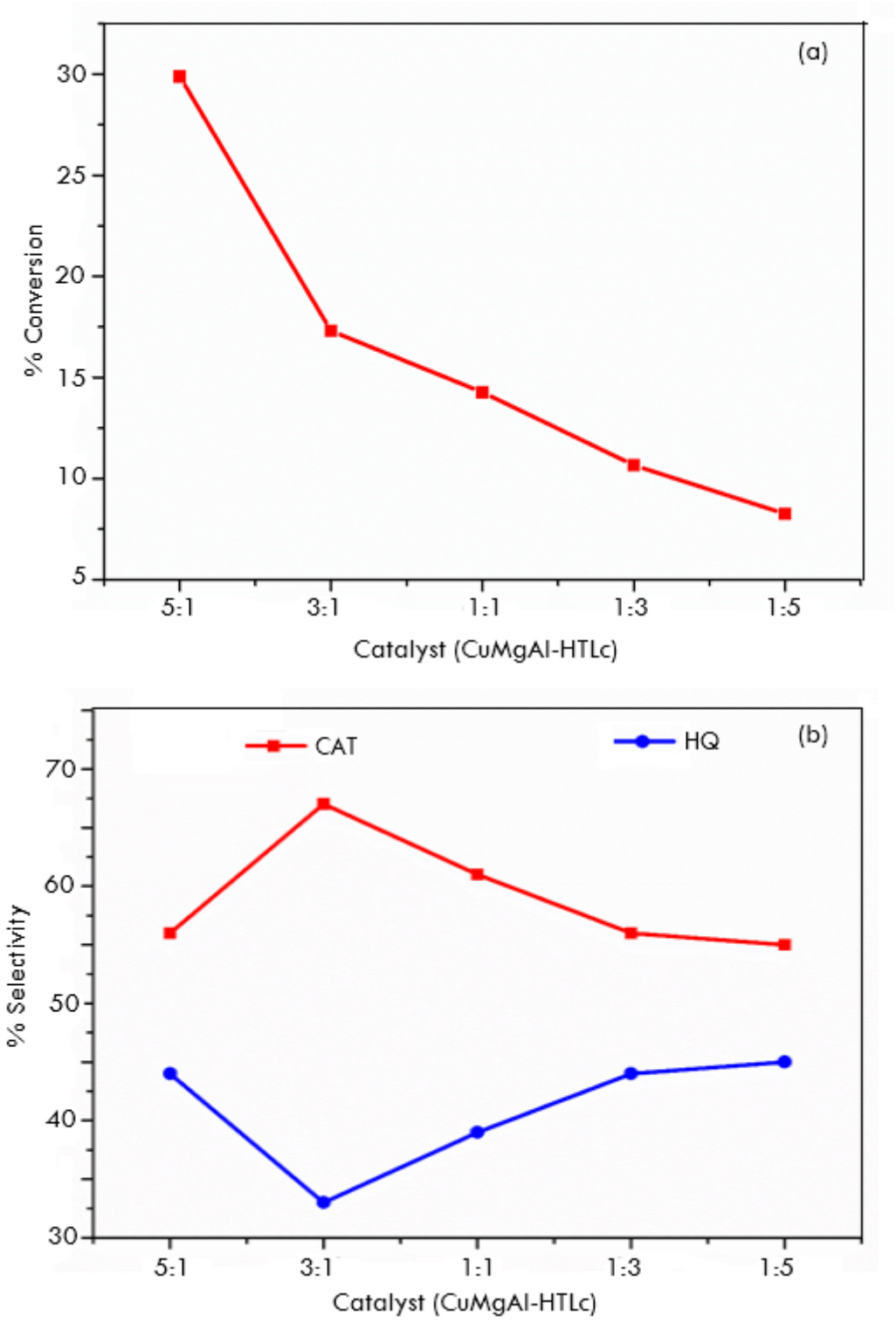

Figure 4.4 Conversion (a) and selectivity (b) over the ternary Cu catalysts

4.3 Proposed reaction pathway

The introduction of copper into the lattice of the hydrotalcite significantly increases the activity of the hydroxylation reaction. It is proposed that in the phenol hydroxylation reaction catalyzed by the ternary Cu catalysts, the oxidant H_2O_2 might first adsorb on the surface of the layered structure and receives an electron from Cu^{2+} ions to produce Cu^{3+}, OH^- and the OH radical. The hydroxy radicals might contribute as an electrophile in this reaction and the hydroxy radicals may also be generated through oxidation of Cu^{2+} ions in the HT-lattice by the oxidant H_2O_2. The hydroxyl radicals then attack at ortho and para positions of phenol resulting in the formation of the desired dihydroxybenzenes, catechol and hydroquinone, respectively.

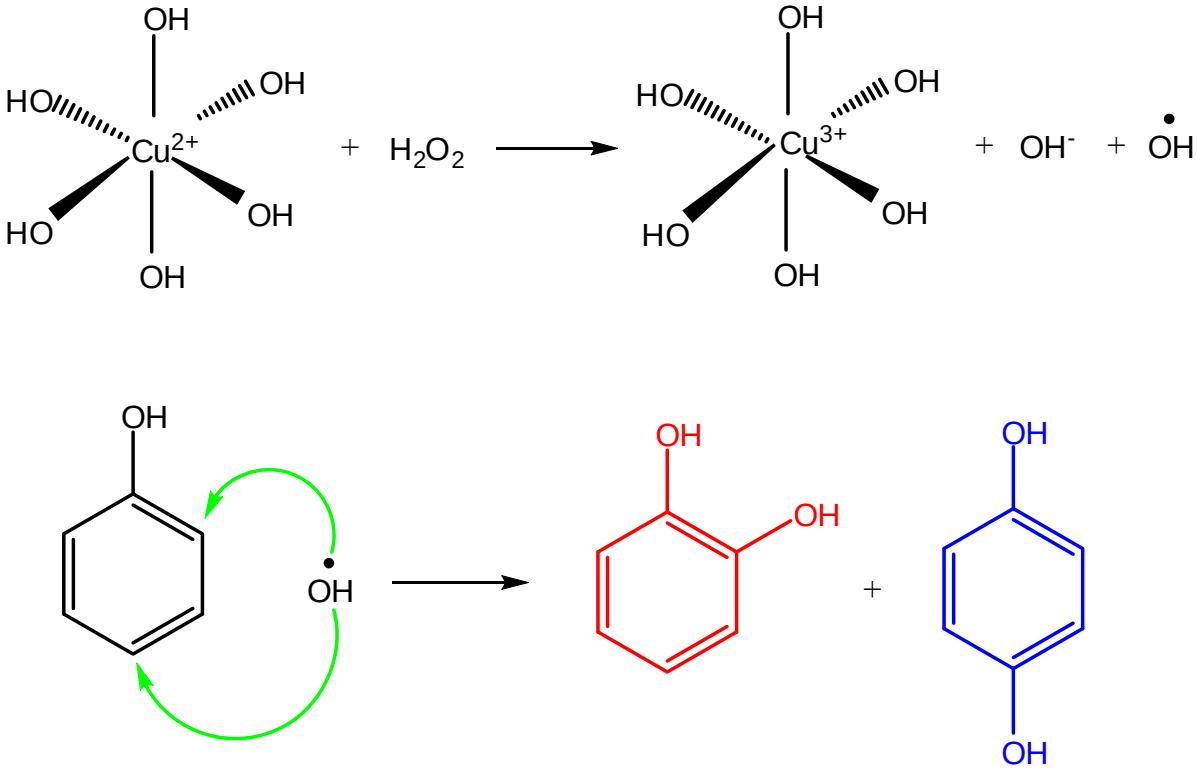

Scheme 4.1. Proposed reaction pathway for phenol hydroxylation over CuMgAl catalysts [94].

CHAPTER FIVE
CONCLUSION

The synthesis of binary and ternary hydrotalcite and hydrotalcite-like compounds was successfully carried out via the co-precipitation method. The success of the synthesis was determined by powder XRD which showed the typical HT characteristic features. The ratio of the two metals, Mg and Al for the HT and the three metals, Cu, Mg and Al for the ternary catalysts determined by ICP-OES were in agreement to the target ratios except for the MgAl-11 which was slightly higher.

The FT-IR spectra of the hydrotalcite and hydrotalcite-like compounds detected the presence of the carbonate ions and water molecules in the interlayer and also the hydroxide groups that made up the brucite-like layers. The detection of these molecules through the presence of their characteristic vibration and stretching bands. The thermal stability of the ternary CuMgAl-31a hydrotalcite-like catalyst and its change in temperature determined by TG-DTA showed the characteristic decomposition behaviour of the removal of water, release of interlay water, dihydroxylation of the hydroxide layers, decarbonisation of the carbonate layers and finally the formation of mixed phase of MgO and $MgAl_2O_4$. The nitrogen isotherms for all the ternary hydrotalcite-like compounds determined by the BET surface area measurements showed the type II isotherms with a relatively small hysteresis loop (Type B). These results were further supported by the pore size distribution. Due to Mg and Al having d^{10} and d^0 electron configurations, respectively, only Cu^{2+} which has d^9 electron configuration was responsible for the bands identified in the UV-Visible spectra. The surface morphology of the ternary hydrotalcite-like compounds and the distribution of the metals, viz. Cu, Mg and Al that were investigated by means of SEM and EDX, respectively, showed that CuMgAl-51a, CuMgAl-31a, and CuMgAl-11a consist of platelets. Overlapping of such platelets arose, thereby exhibiting a spongy morphology. EDX images showed that Cu was homogeneously distributed in all five catalysts with no agglomeration, whereas Mg was randomly distributed.

In the optimization studies, the acetonitrile:ethyl acetate:water (3:3:1) was the best solvent system since it enhanced product isolation and gave the highest conversion. In addition, the triphasic solvent system enhances heterogeneity. Comparison between the solvent systems acetonitrile:ethyl acetate:water (3:3:1), acetonitrile and acetonitrile:water (9:1) with time showed that solvent system acetonitrile:ethyl acetate:water (3:3:1) was the most efficient for a time of 2 hours.

Catalyst loading investigations revealed that 20 mg was the best catalyst loading, a temperature 60°C gave the highest conversion, 2:1 substrate:oxidant ratio was the most appropriate and 10 mL solvent volume was chosen as the optimum.

In the hydroxylation of phenol, blank reactions and testing of the HTs gave minimal conversion. The testing of the ternary catalysts showed improvement in terms of conversion for all the samples. Catechol and hydroquinone were formed as the only products with catechol as a major product. Here, the conversion decreased as the copper concentration decreased and CuMgAl-51a gave the highest phenol conversion of 29.9 % with a 18 % yield of catechol.

The introduction of copper into the lattice of the hydrotalcite significantly increased the activity of the hydroxylation reaction. It was proposed that in the phenol hydroxylation reaction catalyzed by the ternary Cu catalysts, the oxidant H_2O_2 might first adsorb on the surface of the layered structure and receives an electron from Cu^{2+} ions to produce Cu^{3+}, OH^- and the OH radical. The hydroxy radicals might then contribute as an electrophile in this reaction and the hydroxy radicals might also be generated through oxidation of Cu^{2+} ions in the HT-lattice by the oxidant H_2O_2. The hydroxyl radicals then attack at ortho and para positions of phenol resulting in the formation of the desired dihydroxybenzenes, catechol and hydroquinone, respectively.

REFERENCES

[1] T. Degnan Jr., C. Morris Smith and C. Venkat, *Applied Catalysis A: General* **221** (2001) 283–294.

[2] M. Kerby, T. Degnan Jr., D. Marler and J. Beck, *Catalysis Today* **104** (2005) 55–63.

[3] J. Roth, *Catalysis Today* **13** (1992) 1.

[4] J. Zoeller, *Catalysis Today* **140** (2009) 118–126.

[5] M. Twigg, *Applied Catalysis B: Environment* **70** (2007) 2–15.

[6] F. J. Brocker and L. Kainer, German Patent 2,024,282, 1970, to BASF AG and UK Patent 1,342,020, (1971), to BASF AG.

[7] M. I. Fadlalla, An Investigation of a Heterogeneous Aminohydroxylation Catalyst, (2010)

[8] D. Shriver, P. Atkins, Inorganic chemistry, *3rd edition*, (1999) Oxford University Press.

[9] G. C. Bond, Principle of catalysis, the *Chemical Society*, (1972), London.

[10] J. Hagen, Industrial Catalysis: A practical approach, *2nd edition* (2006), Wiley- VCH. Weinheim.

[11] P. G. Jessop, T. Ikariya, R. Noyori, *Chemical Revision,* **99** (1999) 475.

[12] W. R. Barnhart, B. Bosnich, *Organometallics*, **14** (1995) 4343.

[13] J. Xu, A-R Ibrahim, X. Hu, Y. Hong, Y. Su, H Wang, J. Li, *Microporous and Mesoporous Materials,* **231** (2016) 1-8.

[14] F. Shi, L. Mu, P. Yu, J. Hu, L. Zhang, *Journal of Molecular Catalysis A: Chemical* **391** (2014) 66-73.

[15] M. R. Maurya, A. K. Chandrakar, S. Chan, *Journal of Molecular Catalysis A: Chemical* **263** (2007) 227-237.

[16] L. Wang, A. Kong, B. Chen, H. Ding, Y. Shan, M. He, *Journal of Molecular Catalysis A: Chemical* **230** (2005) 143-150.

[17] A. L. Villa, C. A. Laro, C. M. de Correa, *Journal of Molecular Catalysis A: Chemical* **228** (2005) 143-150.

[18] T. Ren, L. Yan, X. Zhang, J. Suo, *Applied Catalysis A: General* **244** (2003) 11-17.

[19] F. Cavani, F. Trifiro, A. Vaccari, Hydrotalcite-type anionic clays: preparation, properties and applications, *Catalysis Today*, **11** (2)(1991) 175-301.

[20] A Vaccari, Preparation and catalytic properties of cationic and anionic clays, *Catalysis Today*, **41** (1998) 53-71.

[21] A. Vaccari, Clays and catalysis: a promising future, *Applied Clay Science*, **14** (1999) 161-198.

[22] C. A. S. Barbosa, P. M. Dias, A. M. da C. Ferreira, V. R. L. Constantino. *Applied Clay Science* **28** (2005) 147-158.

[23] S. Kannan, A. Dubey, H. Knozinger. *Journal of Catalysis* **231** (2005) 381-392.

[24] V. Rives, A. Dubey and S. Kannan. *Journal of Physical Chemistry* **3** (2001) 4826-4836.

[25] B. Balcomb, Layered Double Hydroxides: Synthesis and application in gene delivery to mammalian cells in culture, (2010).

[26] D. Meloni, R. Monaci, V. Solinas, A. Auroux and E. Dumitriu, *Applied Catalysis A: Geneneral*, **350** (2008) 86

[27] H. B. Friedrich and A. S. Mahomed, *Applied Catalysis A: General*, **347** (2008) 11

[28] M. Islam, R. Patel, *Organic-inorganic hybrid ion-exchangers and layered double hydroxides*, Lambert Academic Publishing AG & Co. KG, USA (2009).

[29] B. Li, J. He, D. G. Evans, X. Duan, Inorganic layered double hydroxides as a drug delivery system intercalation and in vitro release of fenbufen, *Applied Clay Science*, **27** (2004) 199-207.

[30] E. Manasse, *American. Social Toscana Science National Pisa PV,* **24** (1915) 92.

[31] N. N. Das, J. Konar, M. K. Mohanta, A. K. Upadhaya, Synthesis, characterization and adsorptive properties of hydrotalcite-like compounds derived from titanium rich bauxite, *Reaction Kinetics Mechanics Catalysis*, **99** (2010) 167-176.

[32] W. Feitknecht, *Helv. Chim. Acta.*,**25** (1942) 131

[33] W. Feitknecht, *Helv. Chim. Acta.*,**25 (**1942) 555

[34] R. Allman, *Chimia*, **24** (1970) 99

[35] H. F. W. Taylor, *Mineral Magazine*, **39** (1973) 377

[36] O. Saber, Preparation and characterization of a new nano-structural material, Co-Sn LDH, *Journal of Physics: Conference Series*, **61** (2007) 825-830.

[37] Z. Janakieva, C. Nachev, D. Yanakieva, Pyroaurite, hydrotalcite and manasseite from Krumovo deposit- new materials for Bulgaria, *Geosciences*, **32**(2007)68-69.

[38] M. L. Kantam, S. Roy, M. Roy, B. Sreedhar, B. M. Choudary, R. L. De, Layered double hydroxides supported rhodium(0): An efficient and reusable catalyst for Heck, Suzuki, and Stille reactions of haloarenes, *Journal of Molecular Catalysis*, **273** (2007) 26-31.

[39] D. G. Cantrell, L. J. Gillie, A. F. Lee, K. Wilson, Structure-reactivity correlations in MgAl hydrotalcite catalysts for biodiesel synthesis, *Applied Catalysis A: General*, **287** (2005) 183-190.

[40] C. T. Chang, B. J. Liaw, C. T. Huang, Y. Z. Chen, Preparation of Au/MgxAlO hydrotalcite catalysts for CO oxidation, *Applied Catalysis A: General*, **332** (2007) 216-224.

[41] Á. Mastalir, Z. Király, Pd nanoparticles in hydrotalcite: mild and highly selective catalysts for alkyne semihydrogenation, *Journal of Catalysis*, **220** (2003) 72-381.

[41] J. S. Valente, J. Hernandez-Cortez, M. S. Cantu, G. Ferrat, E. López-Salinas, Calcined layered double hydroxides Mg–Me–Al (Me: Cu, Fe, Ni, Zn) as bifunctional catalysts, *Catalysis Today*, **150** (2010) 340-345.

[42] D. Kim, C. Huang, H. Lee, I. Han, S. Kang, S. Kwon, J. Lee, Y. Hane, H. Kime, Hydrotalcite-type catalysts for narrow-range oxyethylation of 1-dodecanol using ethyleneoxide, *Applied Catalysis. A: General*, **249** (2003) 229-240.

[43] R. Zăvoianu, R. Bîrjega, O. D. Pavel, A. Cruceanu, M. Alifanti, Hydrotalcite like compounds with low Mo-loading active catalysts for selective oxidation of cyclohexene with hydrogen peroxide, *Applied Catalysi. A: General*, **286** (2005) 211-220.

[44] S. K. Jana, Y. Kubota, T. Tatsumi, High activity of Mn-MgAl hydrotalcite in heterogeneously catalyzed liquid-phase selective oxidation of alkylaromatics to benzylic ketones with 1 atm of molecular oxygen, *Journal of Catalysis*, **247** (2007) 214-222.

[45] D. Kishore, A. E. Rodrigues, Catalytic oxidation of isophorone to ketoisophorone over ruthenium supported MgAl-hydrotalcite, *Catalysis Communication*, **8** (2007) 1156-1160.

[46] K-H. Goha, T. T. Lim, Z. Dong, Application of layered double hydroxides for removal of oxyanions: A review, *Water Research*, **42** (2008) 1343-1368.

[47] T. Bujdosó, Á. Patzkó, Z. Galbács, I. Dékány, Structural characterization of arsenate ion exchanged MgAl-layered double hydroxide, *Applied Clay Science*, **44** (2009) 75-82.

[48] D. M. Roy, R. Roy and E. F. Osborn, *American Journal of Science*, **251 (**1953) 337.

[49] R. Anbarasan, R. Anandhakrishnan, G. Vivek, Synthesis and characterizations of poly(α-naphthylamine)-nanocomposites, *Polymer Composites*, **12** (2008) 949-953.

[50] S. Miyata, *Clays and Clay Minererals*, **31** (1983) 305

[51] S. Gago, M. Pillinger, T. M. Santos, I. S. Gonçalves, Zn-Al layered double hydroxide pillared by different dicarboxylate anions, *Ceramics-Silikáty*, **48** (4)(2004) 155-158.

[52] V. Rives, Layered Double hydroxides: *Present and Future*, Nova Science Publishers, Inc., New York, 2006, p. 1

[53] M. Adachi-Pagano, C. Forano and J.-P. Besse, *Journal of Materials Chemistry*, **13** (2003) 1988.

[54] E. Narita, Y. Matsuno, S. Takahashi and Y. Umetsu, N. K. Kaishi, **49** (2001) 273.

[55] U. Costantino, N. Coletti, M. Nocchetti, G. G. Aloisi, F. Elisei and L. Latterini, *Langmuir*, **16** (2000) 10351.

[56] D. R. Hines, S. A. Solin, U. Costantino and M. Nocchetti, *Physical Review B*, **61** (2000) 11348.

[57] D. R. Hines, S. A. Solin, U. Costantino and M. Nocchetti, *Molecular Crystals and Liquid Crystals*, **341** (2000) 1181.

[58] H. Cai, A. C. Hillier, K. R. Franklin, C. C. Nunn and M. D. Ward, *Science*, **266** (1994) 1551.

[59] F. Prinetto, G. Ghiotti, P. Graffin and D. Tichit, *Microporous and Mesoporous Materials*, **39** (2000) 229.

[60] R. Rosa, C. Leonelli, C. Villa and G. Priarone, *Journal of Microwave Power and Electromagnetic Energy,* **47** (2013) 12.

[61] S. Komarneni, Q. H. Li and R. Roy, *Journal of Materials Research*, **11** (1996) 1866.

[62] K. Ladewig, M. Niebert, Z. P. Xu, P. P. Gray and G. Q. Lu, *Applied Clay Science,* **48** (2010) 280.

[63] M. Li, F. Ni, Y. Wang, S. Xu, D. Zhang and L. Wang, *Applied Clay Science*, **46** (2009) 396.

[64] A. W. Musumeci, G. M. Mortimer, M. K. Butler, Z. P. Xu, R. F. Minchin and D. J. Martin, *Applied Clay Science*, **48** (2010) 271.

[65] D. S. Tong, C. H. Zhou, M. Y. Li, W. H. Yu, J. Beltramini, C. X. Lin and Z. P. Xu, *Applied Clay Science*, **48** (2010) 569.

[66] X. Xie, X. An, K. Yan, X. Wu, J. Song and Z. Wang, *Journal of Natural Gas Chemistry*, **19** (2010) 77.

[67] J. Z. Zhou, Z. P. Xu, S. Qiao, J. Liu, Q. Liu, Y. Xu, J. Zhang and G. Qian, *Applied Clay Science,* **54** (2011) 196.

[68] K. Yan, X. Xie, J. Li, X. Wang and Z. Wang, *Journal of Natural Gas Chemistry*, **16** (2007) 371.

[69] Z. P. Xu, J. Zhang, M. O. Adebajo, H. Zhang and C. Zhou, *Applied Clay Science*, **53** (2011) 139.

[70] H. C. Kolb, M. S. Van Nieuwenhze and K. B. Sharpless, *Chemical Reviews*, **94** (1994) 2483.

[71] G. A. Crispino, K. S. Jeong, H. C. Kolb, Z. M. Wang, D. Q. Xu and K. B. Sharpless, *Journal of Organic Chemistry*, **58** (1993) 3785.

[72] M. K. Tse, K. Schröder and M. Beller, in J. E. Bäckvall (Editor), Modern Oxidation Methods, Vol. 1, 2nd ed., Wiley-VCH Verlag & Co. KGaA., Weinheim, Germany, 2004, p. 1.

[73] G. Lee, J. Y Kanga, N. Yang, Y-W Suhc, J. C. Junga, *Journal of Molecular Catalysis A: Chemical*, **423** (2016) 347–355

[74] M. Bux, Oxidative dehydration of n-octane using vanadium-based hydrotalcite-like compounds, (2010).

[75] K. Zhu, C. Liu, X. Ye and Y. Wu, *Applied Catalysis A.,* **168** (1998) 365

[76] B. M. Choudray, M. L. Kantam, B. Bharathi and C.V. Reddy, *Synlett,***2** (1998)1203

[77] A. Tuel, B. Taarit. *Applied Catalysis A: General* **102** (1993) 69-77.

[78] C. C. Perego, A. P. Ingallina. *Applied Catalysis A: General* **63** (2001) 63-72.

[79] R. Kumar, A. Bhaumik. *Microporous and Mesoporous Material* **21** (1998) 497-504.

[80] D. A. M. Monti, A. Baiker. *Journal of Catalysis,* **83** (1983) 323.

[81] V. V. Potekhin, V. A. Kulikova, V. V. Vasil'ev, E. G. Kohina, V. M. Potekhin. *Russian Journal of Applied Chemistry* **84** (2011) 640-648.

[82] B. Zapata, P. Bosch, G. Fetter, M. A. Valenzuel, J. Navarrete, V. H. Lara, *International Journal of Inorganic Materials*, **3** (2001) 23–29.

[83] D. Kishore and A. E. Rodrigues, *Applied Catalysis A: General* **345** (2008) 104–111.

[84] C. P. Kelkar and A. A. Schutz, *Microporous Materials* **10** (1997) 163 172.

[85] A. A. Schutz, L. A. Cullo and C. P. Kelkar, US Patent 5,399,329 (to Aristech Chemical Corp., Mar. 21, 1995).

[86] C. P. Kelkar, A. A. Schutz and L. A. Cullo, US Patent, 5,518,704 (to Aristech Chemical Corp., Mar. 2l, 1996).

[87] C. Xia, L. Long, B. Zhu, M. Lin, X. Shub, *Catalysis Communications* **80** (2016) 49–52.

[88] C. J. Serna, J. L. Rendon, J. E. Iglesias, Crystal-chemical study of layered $[Al_2Li(OH)_6]^+X^-.nH_2O$, *Clays and Clay Minerals*, **30** (3)(1982) 180-184.

[89] F. Millange, R. I. Walton, D. O'Hare, Time resolved in situ x-ray diffraction study of the liquid-phase reconstruction of Mg-Al-carbonate hydrotalcite-like compounds, *Journal of Material Chemistry*, **10** (2000) 1713-1720.

[90] H. S. Panda, R. Srivastava, D. Bahadur, Stacking of lamella in Mg/Al hydrotalcites: Effects of metal ion concentrations on morphology, *Material Residue Bulletin*, **43** (2008) 1448-1455.

[91] L. Legrand, G. Sagon, S. Lecomte, A. Chausse, R. Messina, A Raman and infrared study of a new carbonate green rust obtained by electrochemical way, *Corrosion Science*, **43** (2001) 1739-1749.

[92] J. T. Kloprogge, L. Hickey, R. L. Frost, Heating stage Raman and infrared emission spectroscopic study of the dehydroxylation of synthetic Mg-hydrotalcite, *Applied Clay Sciences*, **18** (2001) 37-49.

[93] C. Forano, T. Hibino, F. Leroux and C. Taviot-Guého, in F. Bergaya, B. K. G. Theng and G. Galaxy (Editors), *Handbook of Clay Science,* Vol. 1, Elsevier Science, Amsterdam, 2006, p. 1021.

[94] F. Rouquerol, J. Rouquerol and P. L. Llewellyn, in F. Bergaya, B. K. G. Theng and G. Galaxy (Editors), *Handbook of Clay Science, Vol. 1*, Amsterdam, Elsevier Science, 2006, p. 1003.

APPENDIX 1A

Table 1.1A. Reagents used in preparation of ICP standards

Chemicals	**Supplier/ Manufacturer**
Magnesium nitrate hexahydrate, $Mg(NO_3)_2.6H_2O$, 99% purity	Sigma Aldrich
Aluminium nitrate nonahydrate, $Al(NO_3)_3.9H_2O$, ≥ 98% purity	Sigma Aldrich
Copper nitrate trihydrate, $Cu(NO_3)_2.3H_2O$, > 99% purity	Sigma Aldrich
Hydrochloric acid, HCl, 32% (m/v)	Associated Chemical Enterprises

Synthesis of HTs and LDHs

Calculations of the required amounts of precursors for the synthesis of HTs and LDHs

Preparation of $Mg_6Al_2(OH)_{16}(CO_3^{2-}).4H_2O$ for $x = 0.25$, i.e. Mg:Al = 3:1

$Mg(NO_3)_2.6H_2O$ (0.15 M)

Mm = 256.41 g/mol

Mass of $Mg(NO_3)_2.6H_2O$ required = 0.15 mol × 256.41 g/mol

= 38.46 g

Weighed mass = 38.45 g

$Al(NO_3)_3.9H_2O$ (0.05 M)

Mm = 375.15 g/mol

Mass of $Al(NO_3)_3.9H_2O$ required = 0.05 mol × 375.14 g/mol

= 18.76 g

Weighed mass = 18.78 g

Mm = 105.99 g/mol

Na_2CO_3 (0.125 M) for 500 mL solution

Mass of Na_2CO_3 required = 0.125 mol/L × 0.5 L × 105.99 g/mol

= 6.62 g

Weighed mass = 6.66 g

NaOH (2.0 M) for 250 mL solution

Mm = 40.01 g/mol

Mass of NaOH required = 2 mol/L × 0.25 × 40.01 g/mol

= 20 g

Table 1.2A: Details for the synthesis of binary Mg/Al and ternary Cu-Mg/Al HTLc's

Sample	***x***	**Mass (g)**				
		Cu	**Mg**	**Al**	**Na_2CO_3**	**NaOH**
MgAl-31	0.25	-	38.46	18.76	6.62	20
MgAl-21	0.33	-	25.64	18.76	6.62	20
MgAl-11	0.50	-	12.82	18.76	6.62	20
CuMgAl-51a	0.25	30.81	8.01	23.46	6.62	20
CuMgAl-51b	029	25.55	6.54	23.46	6.62	20
CuMgAl-51c	0.33	25.55	5.42	23.46	6.62	20
CuMgAl-31a	0.25	33.98	12.02	23.46	6.62	20
CuMgAl-31b	029	27.73	9.81	23.46	6.62	20
CuMgAl-31c	0.33	22.99	8.06	23.46	6.62	20
CuMgAl-11a	0.25	22.65	24.04	23.46	6.62	20
CuMgAl-11b	029	18.48	19.62	23.46	6.62	20
CuMgAl-11c	0.33	15.33	16.27	23.46	6.62	20
CuMgAl-13a	0.25	11.33	36.06	23.46	6.62	20
CuMgAl-13b	029	9.24	29.43	23.46	6.62	20
CuMgAl-13c	0.33	7.66	24.40	23.46	6.62	20
CuMgAl-15a	0.25	7.55	40.06	23.46	6.62	20
CuMgAl-15b	029	6.16	32.70	23.46	6.62	20
CuMgAl-15c	0.33	5.11	27.11	23.46	6.62	20

APPENDIX 2A

Calculation of the metal cationic ratio in the Mg/Al binary and Cu-Mg/Al ternary HTLc's using ICP-OES data.

1) Preparation of 5 % HCl (32 % assay) in 1000 mL volumetric flask.

$100\% \rightarrow 1000mL$

$5\% \rightarrow x$

$$x = \frac{5\% \times 1000mL}{100\%}$$

$x = 50mL$

$$\therefore \frac{50mL \times 100\%}{32\%}$$

$= 156mL$

2) Preparation of 100 ppm stock solution of Cu, Mg and Al in 500 mL volumetric flasks.

Cu	Mg	Al
$100mg/L = 0.1g/L$	$100mg/L = 0.1g/L$	$100mg/L = 0.1g/L$
$0.1g \rightarrow 1000mL$	$0.1g \rightarrow 1000mL$	$0.1g \rightarrow 1000mL$
$x \rightarrow 500mL$	$x \rightarrow 500mL$	$x \rightarrow 500mL$
$x = \frac{0.1g \times 500mL}{1000}$	$x = \frac{0.1g \times 500mL}{1000}$	$x = \frac{0.1g \times 500mL}{1000}$
$x = 0.05g$	$x = 0.05g$	$x = 0.05g$
$\frac{0.05g \times 241.6g}{63.55}$	$\frac{0.05g \times 256.41g}{24.31}$	$\frac{0.05g \times 375.14g}{23.98}$
$= 0.1901g$	$= 0.5274g$	$= 0.0.6952g$
Weighed mass = 0.2060 g	weighed mass = 0.5525 g	weighed mass = 0.6908 g

3) Preparation of multi-element working standards of Cu, Mg and Al.

STD 1

Cu	**Mg**	**Al**
$100\,ppm \rightarrow 5\,ppm$	$100\,ppm \rightarrow 5\,ppm$	$100\,ppm \rightarrow 5\,ppm$
$C_1V_1 = C_2V_2$	$C_1V_1 = C_2V_2$	$C_1V_1 = C_2V_2$
$V_1 = \frac{5\,ppm \times 100mL}{100\,ppm}$	$V_1 = \frac{5\,ppm \times 100mL}{100\,ppm}$	$V_1 = \frac{5\,ppm \times 100mL}{100\,ppm}$
$V_1 = 5mL$	$V_1 = 5mL$	$V_1 = 5mL$

STD 2

Cu	**Mg**	**Al**

$100\,ppm \rightarrow 10\,ppm$
$C_1V_1 = C_2V_2$
$V_1 = \frac{10\,ppm \times 100mL}{100\,ppm}$
$V_1 = 10mL$

$100\,ppm \rightarrow 10\,ppm$
$C_1V_1 = C_2V_2$
$V_1 = \frac{10\,ppm \times 100mL}{100\,ppm}$
$V_1 = 10mL$

$100\,ppm \rightarrow 10\,ppm$
$C_1V_1 = C_2V_2$
$V_1 = \frac{10\,ppm \times 100mL}{100\,ppm}$
$V_1 = 10mL$

STD 3

$100\,ppm \rightarrow 15\,ppm$
$C_1V_1 = C_2V_2$
$V_1 = \frac{15\,ppm \times 100mL}{100\,ppm}$
$V_1 = 15mL$

$100\,ppm \rightarrow 15\,ppm$
$C_1V_1 = C_2V_2$
$V_1 = \frac{15\,ppm \times 100mL}{100\,ppm}$
$V_1 = 15mL$

$100\,ppm \rightarrow 15\,ppm$
$C_1V_1 = C_2V_2$
$V_1 = \frac{15\,ppm \times 100mL}{100\,ppm}$
$V_1 = 15mL$

STD 4

$100\,ppm \rightarrow 20\,ppm$
$C_1V_1 = C_2V_2$
$V_1 = \frac{20\,ppm \times 100mL}{100\,ppm}$
$V_1 = 20mL$

$100\,ppm \rightarrow 20\,ppm$
$C_1V_1 = C_2V_2$
$V_1 = \frac{20\,ppm \times 100mL}{100\,ppm}$
$V_1 = 20mL$

$100\,ppm \rightarrow 20\,ppm$
$C_1V_1 = C_2V_2$
$V_1 = \frac{20\,ppm \times 100mL}{100\,ppm}$
$V_1 = 20mL$

STD 5

$100\,ppm \rightarrow 25\,ppm$
$C_1V_1 = C_2V_2$
$V_1 = \frac{25\,ppm \times 100mL}{100\,ppm}$
$V_1 = 25mL$

$100\,ppm \rightarrow 25\,ppm$
$C_1V_1 = C_2V_2$
$V_1 = \frac{25\,ppm \times 100mL}{100\,ppm}$
$V_1 = 25mL$

$100\,ppm \rightarrow 25\,ppm$
$C_1V_1 = C_2V_2$
$V_1 = \frac{25\,ppm \times 100mL}{100\,ppm}$
$V_1 = 25mL$

Table 2.1A. Parameters that provided optimum calibration profile for each element.

Element	Mass (g)	Wavelength (nm)	r^2
Cu	0.2060	324.754	0.9999
Mg	0.5525	383.231	0.9999
Al	0.6908	394.403	0.9999

Table 2.2A. Preparation of multi-element working standards containing Cu, Mg and Al cations

Standard	Volume (mL)	Concentration (ppm)		
		Cu	Mg	Al
1	5	5	5	5
2	10	10	10	10
3	15	15	15	15
4	20	20	20	20
5	25	25	25	25

Table 2.3A: Weighed masses of the binary and ternary HTLc's

Sample	*x*	Weighed mass (g)
MgAl-31	0.25	0.0122
MgAl-21	0.33	0.0118
MgAl-11	0.50	0.0103
CuMgAl-51a	0.25	0.0120
CuMgAl-51b	0.29	0.0132
CuMgAl-51c	0.33	0.0101
CuMgAl-31a	0.25	0.0103
CuMgAl-31b	0.29	0.0117
CuMgAl-31c	0.33	0.0168
CuMgAl-11a	0.25	0.0103
CuMgAl-11b	0.29	0.0111
CuMgAl-11c	0.33	0.0102
CuMgAl-13a	0.25	0.0147
CuMgAl-13b	0.29	0.0100
CuMgAl-13c	0.33	0.0104
CuMgAl-15a	0.25	0.0143
CuMgAl-15b	0.29	0.0105
CuMgAl-15c	0.33	0.0132

Molar cationic ratio calculations from the ICP-OES data

CuMgAl=51a

Cu	**Mg**	**Al**
$m = 66.6mg/L \times 0.1L$	$m = 6.46mg/L \times 0.1L$	$m = 8.57mg/L \times 0.1L$
$m = 6.66mg = 0.00666g$	$m = 0.646mg = 0.000646g$	$m = 0.857mg = 0.000857g$
$m = 66.6g(\times 10000dilution)$	$m = 6.46g(\times 10000dilution)$	$m = 8.57g(\times 10000dilution)$
$n = \frac{66.6g}{63.55g/mol}$	$n = \frac{6.46g}{24.31g/mol}$	$n = \frac{8.57g}{26.98g/mol}$
$n = 1.04799mol$	$n = 0.2161mol$	$n = 0.4158mol$

Cu/Mg = 4.85 and (Cu + Mg)/Al = 3.04

CuMgAl-51b

Cu	**Mg**	**Al**
$m = 45.6mg/L \times 0.1L$	$m = 4.00mg/L \times 0.1L$	$m = 9.55mg/L \times 0.1L$
$m = 4.56mg = 0.00456g$	$m = 0.400mg = 0.000400g$	$m = 0.955mg = 0.000955g$
$m = 45.6g(\times 10000dilution)$	$m = 4.00g(\times 10000dilution)$	$m = 9.55g(\times 10000dilution)$
$n = \frac{45.6g}{63.55g/mol}$	$n = \frac{4.00g}{24.31g/mol}$	$n = \frac{9.55g}{26.98g/mol}$
$n = 0.7175mol$	$n = 0.1486mol$	$n = 0.3594mol$

Cu/Mg = 4.83 and (Cu + Mg)/Al = 2.41

CuMgAl-51c

$m = 54.9mg/L \times 0.1L$	$m = 4.64mg/L \times 0.1L$	$m = 12.1mg/L \times 0.1L$
$m = 5.49mg = 0.00549g$	$m = 0.464mg = 0.000464g$	$m = 1.21mg = 0.00121g$
$m = 54.9g(\times 10000dilution)$	$m = 4.64g(\times 10000dilution)$	$m = 12.1g(\times 10000dilution)$
$n = \frac{54.9g}{63.55g/mol}$	$n = \frac{4.64g}{24.31g/mol}$	$n = \frac{12.1g}{26.98g/mol}$
$n = 0.8639mol$	$n = 0.1728mol$	$n = 0.5183mol$

Cu/Mg = 5.00 and (Cu + Mg)/Al = 2.00

CuMgAl-31a

$m = 33.1 mg/L \times 0.1L$ $m = 4.45 mg/L \times 0.1L$ $m = 6.63 mg/L \times 0.1L$

$m = 3.31 mg = 0.00331 g$ $m = 0.445 mg = 0.000445 g$ $m = 0.663 mg = 0.000663 g$

$m = 33.1 g (\times 10000 dilution)$ $m = 4.45 g (\times 10000 dilution)$ $m = 6.63 g (\times 10000 dilution)$

$n = \frac{33.1 g}{63.55 g/mol}$ $n = \frac{4.45 g}{24.31 g/mol}$ $n = \frac{6.63 g}{26.98 g/mol}$

$n = 0.5208 mol$ $n = 0.1765 mol$ $n = 0.2324 mol$

Cu/Mg = 2.95 and (Cu + Mg)/Al = 3.00

CuMgAl-31b

$m = 41.0 mg/L \times 0.1L$ $m = 5.49 mg/L \times 0.1L$ $m = 8.74 mg/L \times 0.1L$

$m = 4.10 mg = 0.00410 g$ $m = 0.549 mg = 0.000549 g$ $m = 0.874 mg = 0.000874 g$

$m = 41.0 g (\times 10000 dilution)$ $m = 5.49 g (\times 10000 dilution)$ $m = 8.74 g (\times 10000 dilution)$

$n = \frac{41.0 g}{63.55 g/mol}$ $n = \frac{5.49 g}{24.31 g/mol}$ $n = \frac{8.74 g}{26.98 g/mol}$

$n = 0.6452 mol$ $n = 0.2195 mol$ $n = 0.3529 mol$

Cu/Mg = 2.94 and (Cu + Mg)/Al = 2.45

CuMgAl-31c

Cu **Mg** **Al**

$m = 38.1 mg/L \times 0.1L$ $m = 5.65 mg/L \times 0.1L$ $m = 10.6 mg/L \times 0.1L$

$m = 38.1 mg = 0.00381 g$ $m = 0.0565 mg = 0.000565 g$ $m = 1.06 mg = 0.00106 g$

$m = 38.1 g (\times 10000 dilution)$ $m = 5.65 g (\times 10000 dilution)$ $m = 1.06 g (\times 10000 dilution)$

$n = \frac{38.1 g}{63.55 g/mol}$ $n = \frac{5.65 g}{24.31 g/mol}$ $n = \frac{10.6 g}{26.98 g/mol}$

$n = 0.5995 mol$ $n = 0.1998 mol$ $n = 0.4120 mol$

Cu/Mg = 3.00 and (Cu + Mg)/Al = 1.94

CuMgAl-11a

$m = 28.6 mg/L \times 0.1L$ $m = 9.78 mg/L \times 0.1L$ $m = 8.24 mg/L \times 0.1L$

$m = 2.86 mg = 0.00286 g$ $m = 0.978 mg = 0.000978 g$ $m = 0.824 mg = 0.000824 g$

$m = 28.6 g (\times 10000 dilution)$ $m = 9.78 g (\times 10000 dilution)$ $m = 8.24 g (\times 10000 dilution)$

$n = \frac{28.6 g}{63.55 g/mol}$ $n = \frac{9.78 g}{24.31 g/mol}$ $n = \frac{8.24 g}{26.98 g/mol}$

$n = 0.4500 mol$ $n = 0.4639 mol$ $n = 0.3046 mol$

Cu/Mg = 0.97 and (Cu + Mg)/Al = 3.00

CuMgAl-11b

$m = 26.9mg/L \times 0.1L$	$m = 10.4mg/L \times 0.1L$	$m = 8.86mg/L \times 0.1L$
$m = 2.69mg = 0.00269g$	$m = 1.04mg = 0.00104g$	$m = 0.886mg = 0.000886g$
$m = 26.9g(\times 10000dilution)$	$m = 10.4g(\times 10000dilution)$	$m = 8.86g(\times 10000dilution)$
$n = \frac{26.9g}{63.55g/mol}$	$n = \frac{10.4g}{24.31g/mol}$	$n = \frac{8.86g}{26.98g/mol}$
$n = 0.4233mol$	$n = 0.4110mol$	$n = 0.3505mol$

Cu/Mg = 1.03 and (Cu + Mg)/Al = 2.38

CuMgAl-11c

$m = 21.6mg/L \times 0.1L$	$m = 8.77mg/L \times 0.1L$	$m = 10.0mg/L \times 0.1L$
$m = 2.16mg = 0.00216g$	$m = 0.877mg = 0.000877g$	$m = 1.00mg = 0.00100g$
$m = 21.6g(\times 10000dilution)$	$m = 8.77g(\times 10000dilution)$	$m = 10.0g(\times 10000dilution)$
$n = \frac{21.6g}{63.55g/mol}$	$n = \frac{8.77g}{24.31g/mol}$	$n = \frac{10.0g}{26.98g/mol}$
$n = 0.4500mol$	$n = 0.4639mol$	$n = 0.4502mol$

Cu/Mg = 0.97 and (Cu + Mg)/Al = 2.03

CuMgAl-13a

Cu	**Mg**	**Al**
$m = 15.5mg/L \times 0.1L$	$m = 15.2mg/L \times 0.1L$	$m = 9.14mg/L \times 0.1L$
$m = 1.55mg = 0.00155g$	$m = 1.52mg = 0.00152g$	$m = 0.914mg = 0.000914g$
$m = 15.5g(\times 10000dilution)$	$m = 1.52g(\times 10000dilution)$	$m = 9.14g(\times 10000dilution)$
$n = \frac{15.5g}{63.55g/mol}$	$n = \frac{1.52g}{24.31g/mol}$	$n = \frac{9.14g}{26.98g/mol}$
$n = 0.2352mol$	$n = 0.6689mol$	$n = 0.3014mol$

Cu/Mg = 0.34 and (Cu + Mg)/Al = 3.00

CuMgAl-13b

$m = 16.0mg/L \times 0.1L$ $m = 17.8mg/L \times 0.1L$ $m = 11.0mg/L \times 0.1L$

$m = 1.60mg = 0.00160g$ $m = 1.78mg = 0.00178g$ $m = 1.10mg = 0.00110g$

$m = 16.0g(\times 10000dilution)$ $m = 17.8g(\times 10000dilution)$ $m = 11.0g(\times 10000dilution)$

$n = \frac{16.0g}{63.55g/mol}$ $n = \frac{17.8g}{24.31g/mol}$ $n = \frac{11.0g}{26.98g/mol}$

$n = 0.2518mol$ $n = 0.7322mol$ $n = 0.4077mol$

Cu/Mg = 0.34 and (Cu + Mg)/Al = 2.45

CuMgAl-13c

$m = 21.3mg/L \times 0.1L$ $m = 24.1mg/L \times 0.1L$ $m = 18.8mg/L \times 0.1L$

$m = 2.13mg = 0.002.13g$ $m = 2.41mg = 0.00241g$ $m = 1.88mg = 0.00188g$

$m = 21.3g(\times 10000dilution)$ $m = 24.1g(\times 10000dilution)$ $m = 18.8g(\times 10000dilution)$

$n = \frac{21.3g}{63.55g/mol}$ $n = \frac{24.1g}{24.31g/mol}$ $n = \frac{18.8g}{26.98g/mol}$

$n = 0.3375mol$ $n = 0.9914mol$ $n = 0.6968mol$

Cu/Mg = 0.33 and (Cu + Mg)/Al= 1.94

CuMgAl-15a

$m = 11.6mg/L \times 0.1L$ $m = 21.7mg/L \times 0.1L$ $m = 9.76mg/L \times 0.1L$

$m = 1.16mg = 0.00116g$ $m = 21.7mg = 0.0021.7g$ $m = 0.976mg = 0.00097g$

$m = 11.6g(\times 10000dilution)$ $m = 21.7g(\times 10000dilution)$ $m = 9.76g(\times 10000dilution)$

$n = \frac{11.6g}{63.55g/mol}$ $n = \frac{21.7g}{24.31g/mol}$ $n = \frac{9.76g}{26.98g/mol}$

$n = 0.1747mol$ $n = 0.8926mol$ $n = 0.3550mol$

Cu/Mg = 0.21 and (Cu + Mg)/Al = 3.04

CuMgAl-15b

Cu **Mg** **Al**

$m = 11.9mg/L \times 0.1L$ $m = 22.8mg/L \times 0.1L$ $m = 12.6mg/L \times 0.1L$

$m = 1.19mg = 0.00119g$ $m = 2.28mg = 0.00228g$ $m = 1.26mg = 0.00126g$

$m = 11.9g(\times 10000dilution)$ $m = 22.8g(\times 10000dilution)$ $m = 12.6g(\times 10000dilution)$

$n = \frac{11.9g}{63.55g/mol}$ $n = \frac{22.8g}{24.31g/mol}$ $n = \frac{12.6g}{26.98g/mol}$

$n = 0.1873mol$ $n = 0.9379mol$ $n = 0.4670mol$

Cu/Mg = 0.20 and (Cu + Mg)/Al = 2.41

CuMgAl-15c

$m = 9.00 mg/L \times 0.1 L$	$m = 17.6 mg/L \times 0.1 L$	$m = 11.7 mg/L \times 0.1 L$
$m = 0.9 mg = 0.0009 g$	$m = 1.76 mg = 0.00176 g$	$m = 1.17 mg = 0.00117 g$
$m = 9 g (\times 10000 dilution)$	$m = 17.6 g (\times 10000 dilution)$	$m = 11.7 g (\times 10000 dilution)$
$n = \frac{9 g}{63.55 g/mol}$	$n = \frac{17.6 g}{24.31 g/mol}$	$n = \frac{11.7 g}{26.98 g/mol}$
$n = 0.1416 mol$	$n = 0.7220 mol$	$n = 0.4337 mol$

Cu/Mg = 0.20 and (Cu + Mg)/Al = 2.00

APPENDIX 3A

Calculations of the *a* parameter

a parameter = $2d_{110}$

where d = d-basal spacing of the first peak in the 110 plane

Binary MgAl-31

$a = 2 \times 1.52$

$= \underline{3.04}$

Calculations of the *c* parameter

$c = 3/2\ [d_{003} + 2d_{006}]$

Binary MgAl-31

$c = 3/2\ [7.67 + 2(3.87)]$

$= \underline{23.18}$

Table 3.1A: d-basal spacing values, *a* and *c* parameters for the binary MgAl and ternary Cu-Mg/Al HTLcs

Sample	**Basal spacing (Å)**			**a**	**c**
	d_{003}	**d_{006}**	**d_{110}**		
MgAl-31	7.67	3.87	1.52	3.04	23.18
MgAl-21	7.41	3.75	1.52	3.03	22.38
MgAl-11	7.43	3.75	1.51	3.02	22.39
CuMgAl-51a	7.50	3.77	1.53	3.06	22.55
CuMgAl-31a	7.58	3.75	1.55	3.09	22.61
CuMgAl-11a	7.61	3.81	1.54	3.08	22.84
CuMgAl-13c	7.72	3.78	1.54	3.08	22.92
CuMgAl-15b	7.73	3.82	1.54	3.07	23.05

APPENDIX 4A

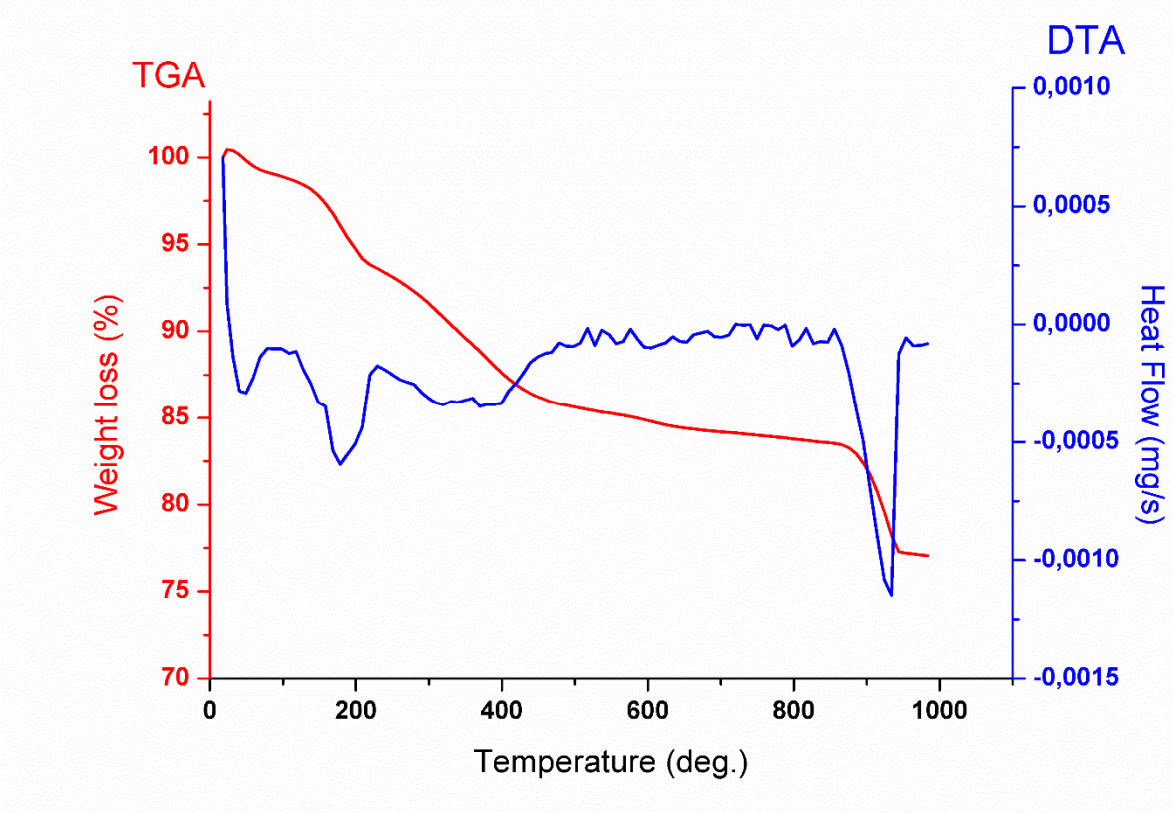

Figure 4.1A. TG-DTA of ternary CuMgAl-51a HTLc

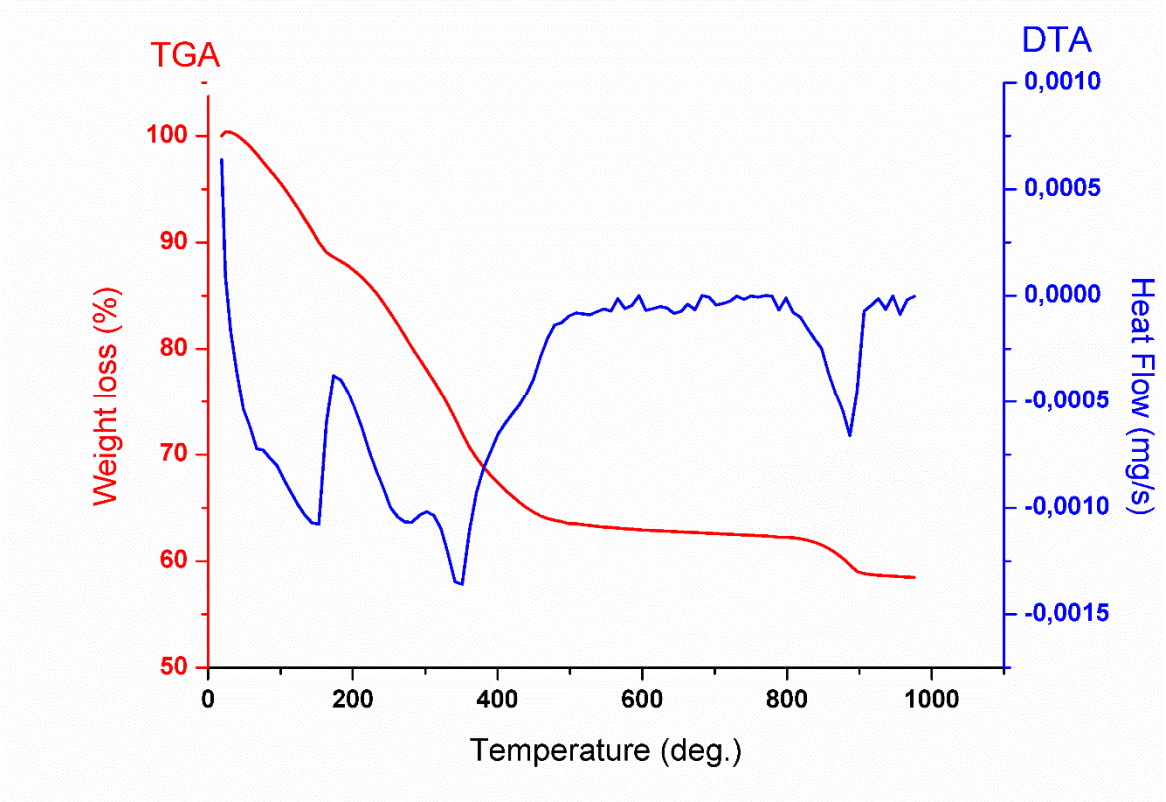

Figure 4.2A. TG-DTA of ternary CuMgAl-11a HTLc

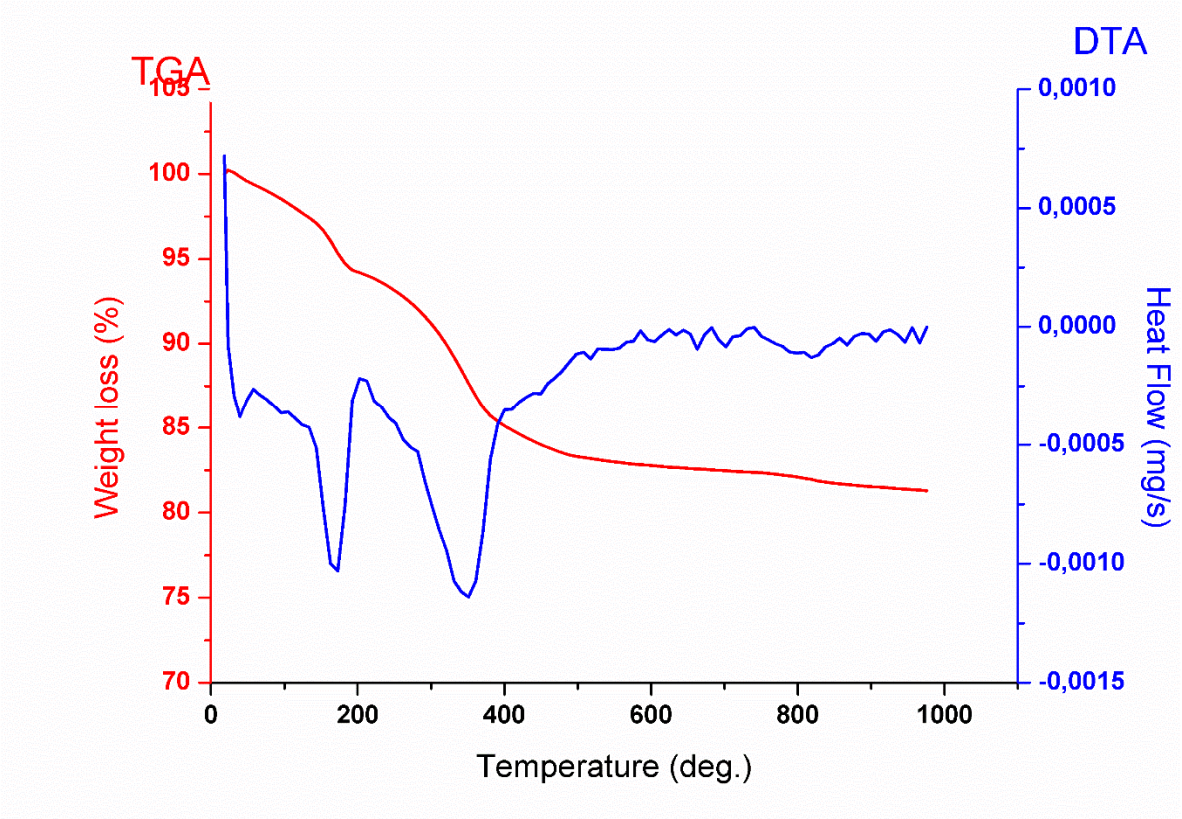

Figure 4.3A. TG-DTA of ternary CuMgAl-13 HTLc

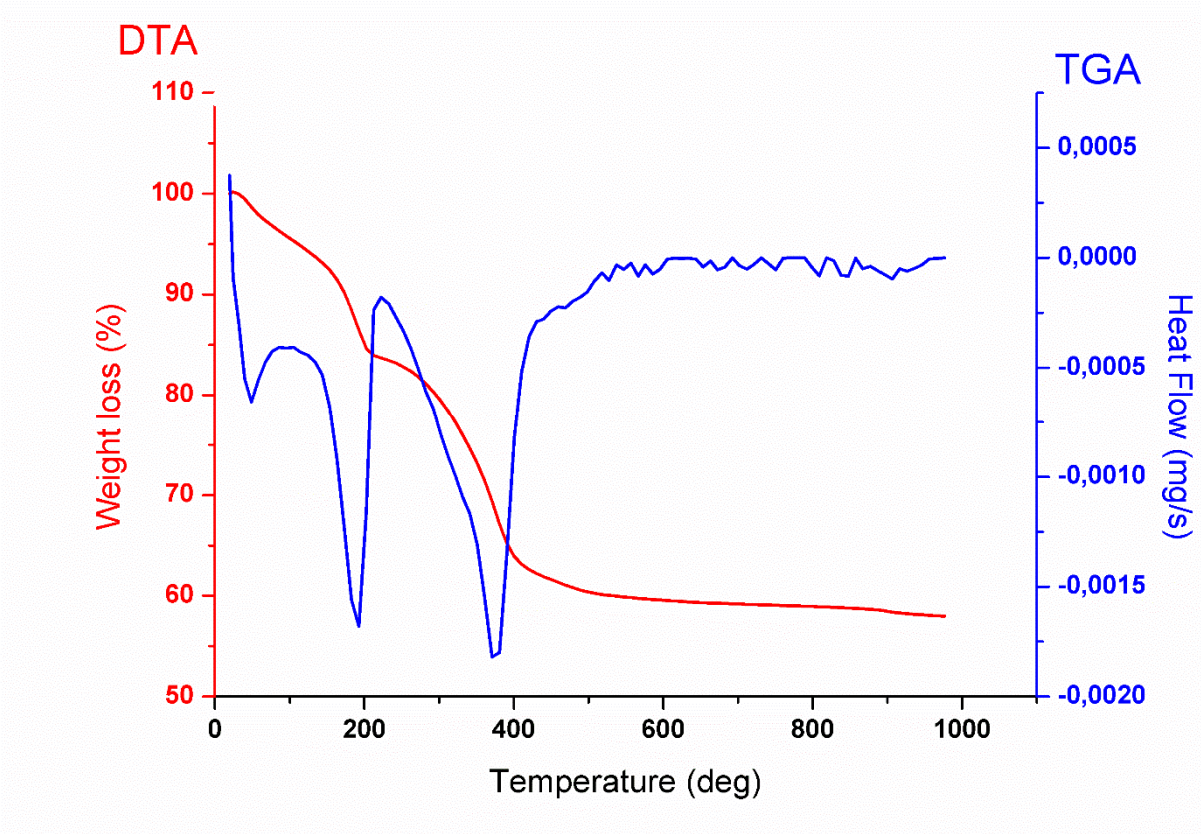

Figure 4.4A. TG-DTA of ternary CuMgAl-15b HTLc

APPENDIX 5A

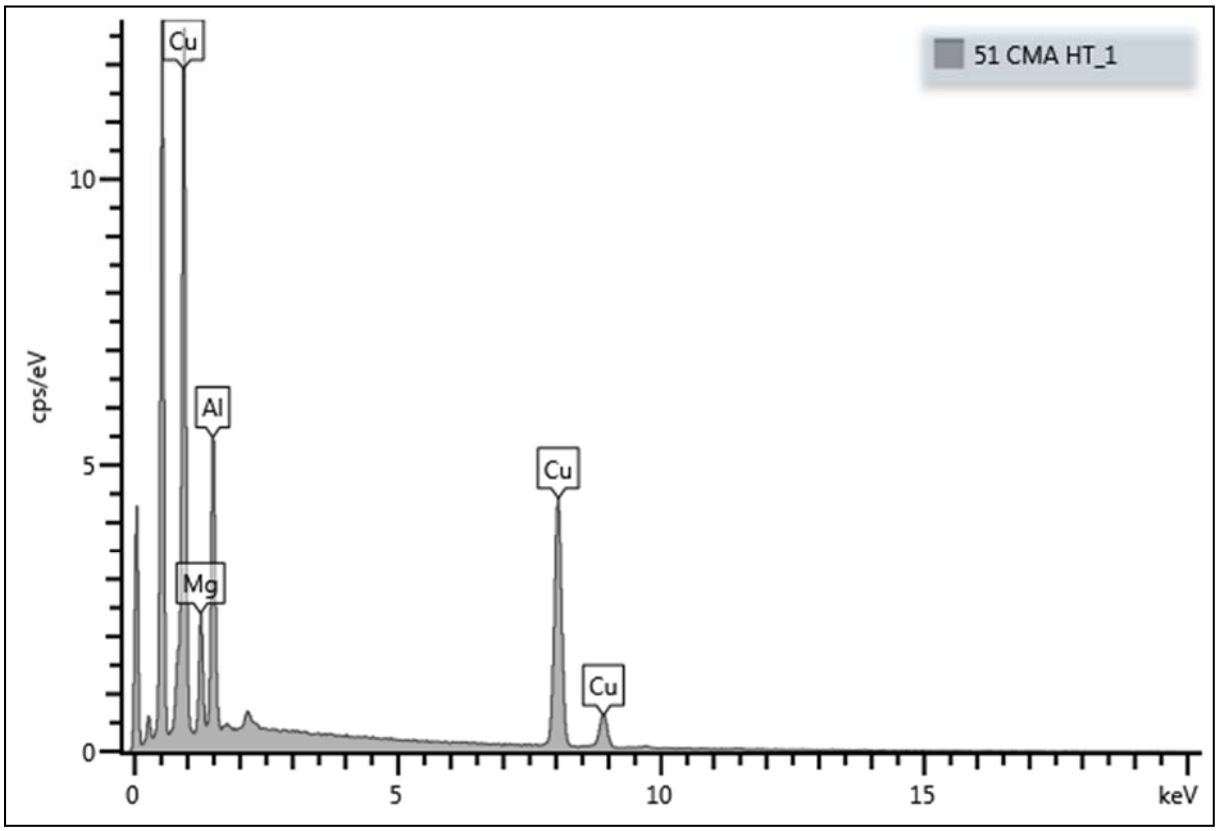

Figure 5.1A. SEM-EDX spectrum for CuMgAl-51a

Table 5.1A: SEM-EDX elemental data for CuMgAl-51a.

51 CMA HT_1	Atomic %	51 CMA HT_1	Wt%	Wt% Sigma
Mg	18.98	Mg	10.59	0.20
Al	34.25	Al	21.21	0.22
Cu	46.77	Cu	68.20	0.27
Total	100.00	Total	100.00	

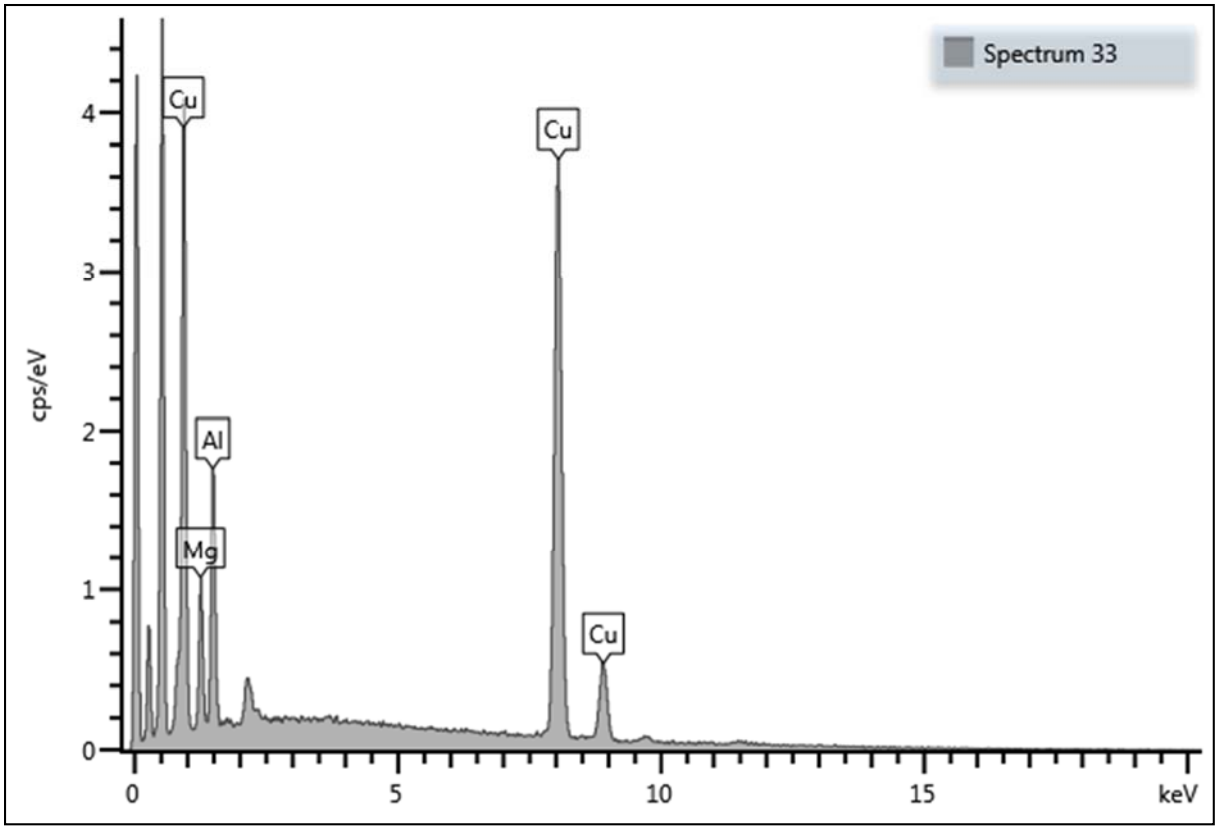

Figure 5.2A. SEM-EDX spectrum for CuMgAl-31a

Table 5.2A: SEM-EDX elemental data for CuMgAl-31a.

31 CMA HT_1	Atomic %	31 CMA HT_1	Wt%	Wt% Sigma
Mg	16.24	Mg	7.91	0.22
Al	19.93	Al	10.78	0.21
Cu	63.83	Cu	81.30	0.29
Total	100.00	Total	100.00	

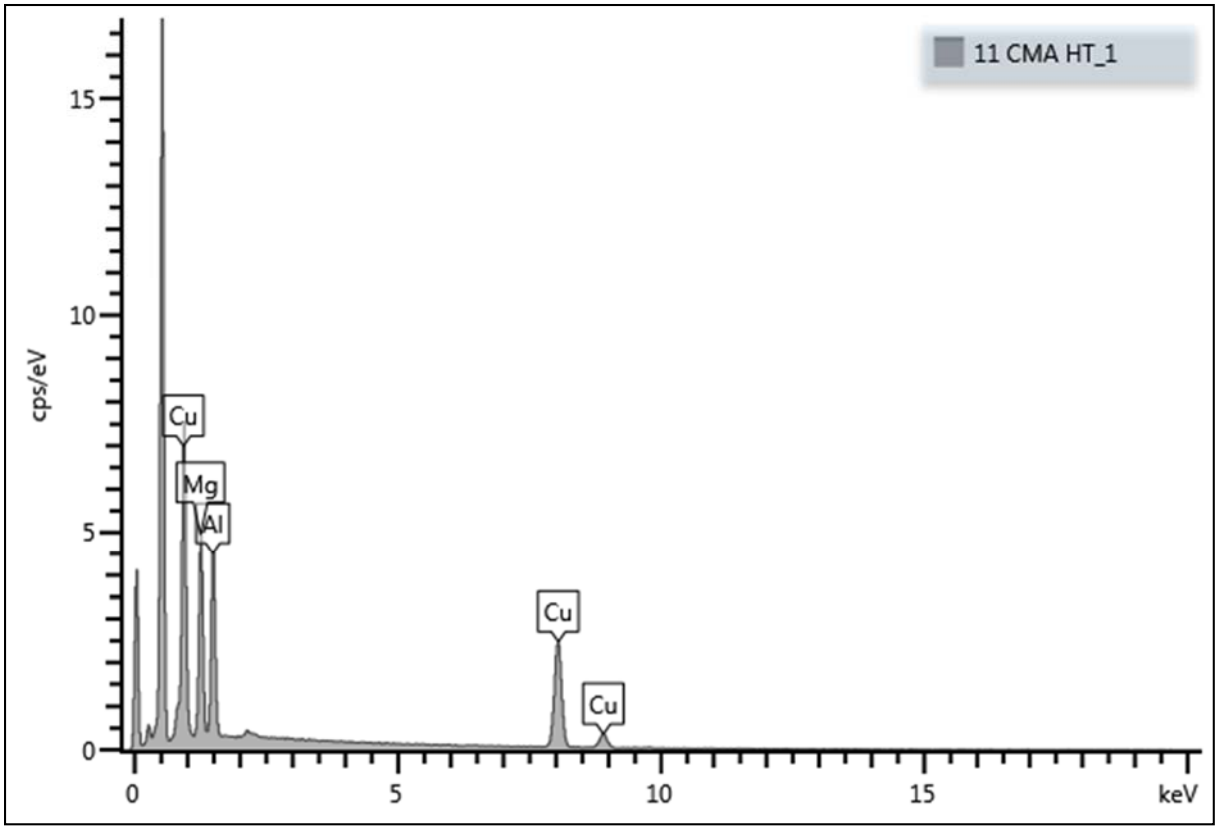

Figure 5.3A. SEM-EDX spectrum for CuMgAl-11a

Table 5.3A: SEM-EDX elemental data for CuMgAl-11a.

11 CMA HT_1	Atomic %	11 CMA HT_1	Wt%	Wt% Sigma
Mg	38.19	Mg	25.09	0.27
Al	31.59	Al	23.03	0.26
Cu	30.22	Cu	51.88	0.33
Total	100.00	Total	100.00	

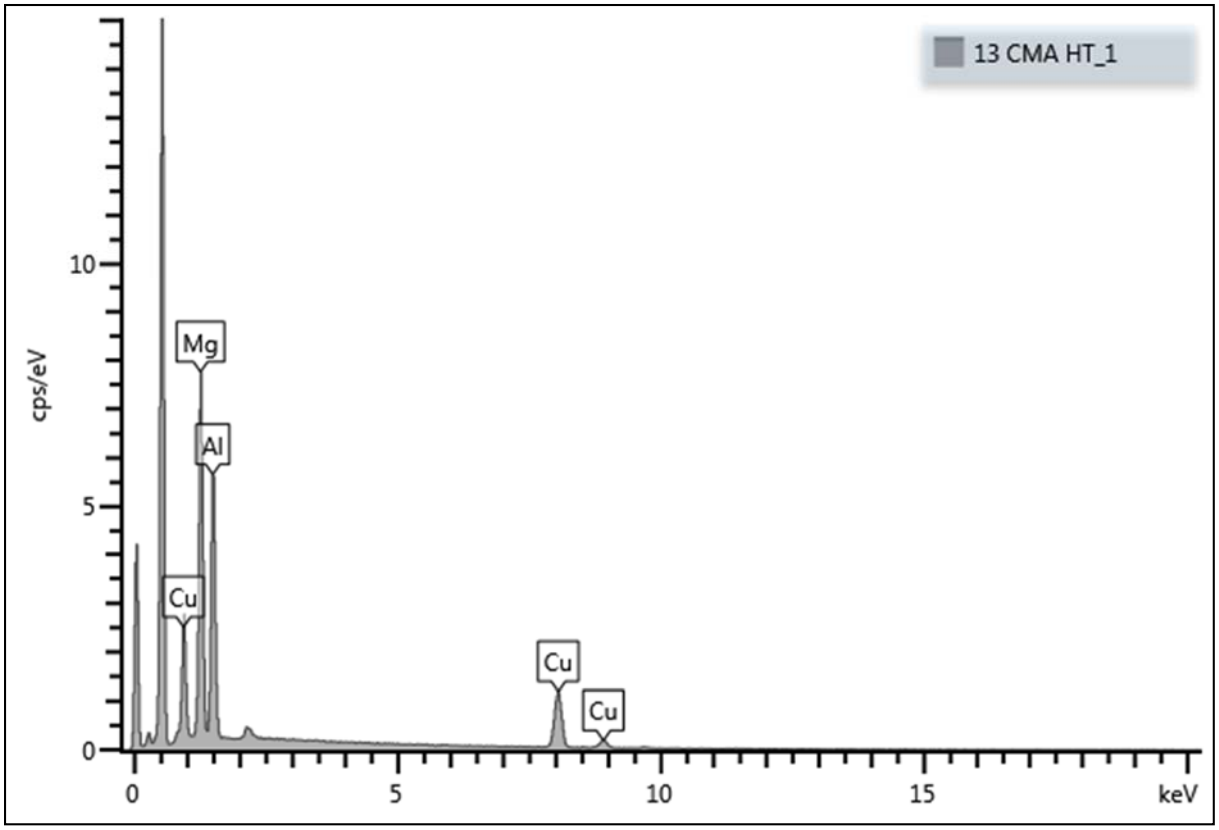

Figure 5.4A. SEM-EDX spectrum for CuMgAl-13c

Table 5.4A: SEM-EDX elemental data for CuMgAl-13c.

13 CMA HT_1	Atomic %	13 CMA HT_1	Wt%	Wt% Sigma
Mg	45.74	Mg	35.37	0.30
Al	38.72	Al	33.23	0.30
Cu	15.54	Cu	31.40	0.37
Total	100.00	Total	100.00	

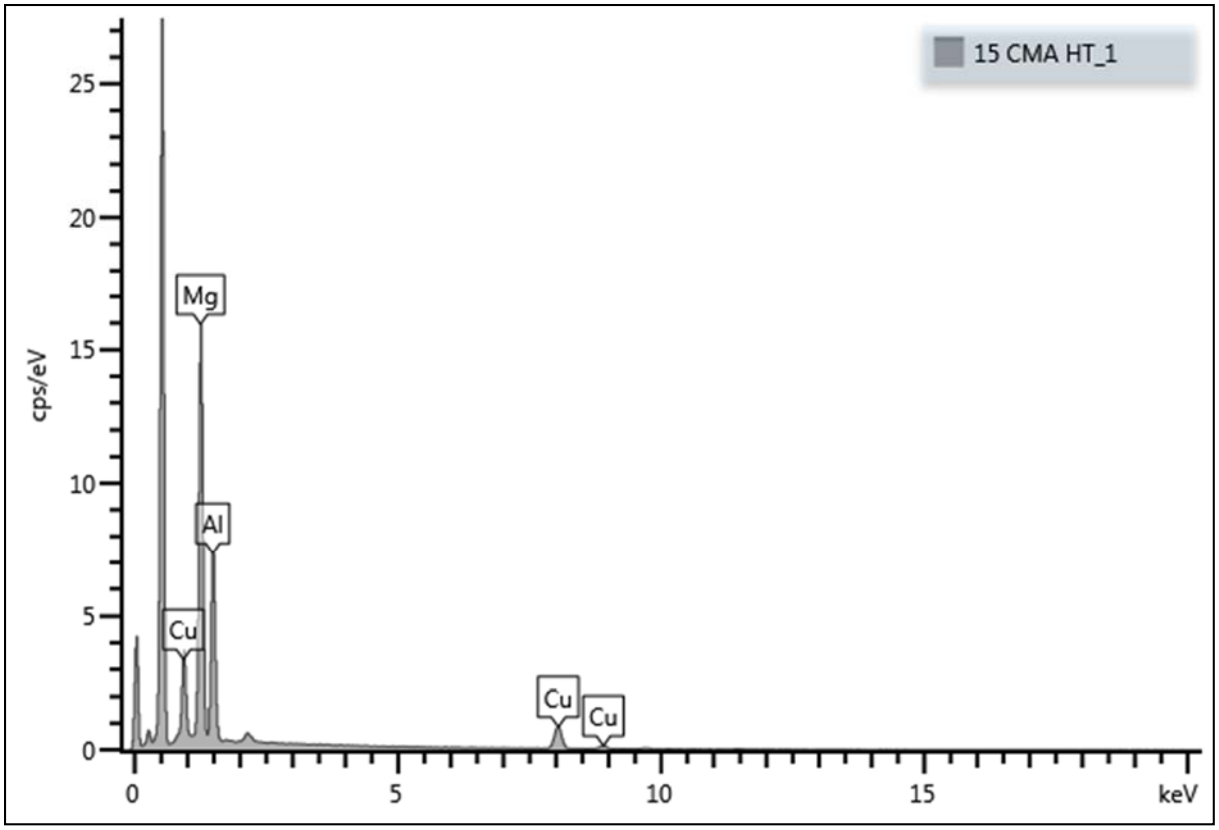

Figure 5.5A. SEM-EDX spectrum for CuMgAl-15b

Table 5.5A: SEM-EDX elemental data for CuMgAl-15b.

15 CMA HT_1	Atomic %	15 CMA HT_1	Wt%	Wt% Sigma
Mg	54.59	Mg	46.31	0.27
Al	36.84	Al	34.68	0.27
Cu	8.57	Cu	19.01	0.30
Total	100.00	Total	100.00	

APPENDIX 6A

Table 6.1A. Optimized gas chromatograph method and column specifications

Oven Temperature, (ºC)		
Initial temperature: 160	Maximum temperature: 240	
Temperature Programme		
Temperature, (ºC)	Ramp, (ºC/min)	Hold time, (min)
160	-	-
205	50	2
240	15	6
Front Inlet		
Mode	Split	
Ratio	100.0	
Temperature	200 ºC	
Gas type	Hydrogen and air	
Flow rate	1.25 mL/min	
Column		
Name	ZB-WAX PLUS (30.0 m × 0.25 mm × 0.25 μm)	
Detector		
Name	Flame Ionization Detector	
Temperature	250 ºC	

Table 6.2A. effect of temperature investigations on binary MgAl HTs

Sample	Temperature, (^{o}C)	Conversion, (%)	Product distribution, (%)	
			CAT	HQ
MgAl-31	30	0.48	20	80
	60	0.88	7	93
	80	0.61	6	94
MgAl-21	30	0.55	17	83
	60	0.82	21	79
	80	0.73	24	76
MgAl-11	30	0.62	17	83
	60	0.81	4	96
	80	0.69	17	83

Table 6.3A. Influence of substrate oxidant ratio over binary MgAl HTs

Sample	Substrate/Oxidant ratio	Conversion, (%)	Product distribution, (%)	
			CAT	HQ
MgAl-31	3:1	0.77	0	100
	2:1	0.84	7	93
	1:1	0.86	4	96
MgAl-21	3:1	0.66	13	87
	2:1	0.75	21	79
	1:1	0.81	15	85
MgAl-11	3:1	0.80	17	83
	2:1	0.85	4	96
	1:1	0.92	20	80

Table 6.4A: Hydroxylation of phenol activity of all synthesized CuMgAl ternary HTLcs.

HTlca	Cu/Mg	x	(Cu+Mg)/Aℓ	Phenol Conversion, (%)	Product distribution, (%)		
					CAT	HQ	CAT/HQ
1	5:1	0.25	3:1	29.9	56	44	1.3
2		0.29	2.4:1	18.6	62	38	1.6
3		0.33	2:1	11.6	60	40	1.5
4	3:1	0.25	3:1	17.3	67	33	1.8
5		0.29	2.4:1	10.2	60	40	1.5
6		0.33	2:1	5.1	62	38	1.6
7	1:1	0.25	3:1	14.3	61	39	1.6
8		0.29	2.4:1	13.2	53	47	1.1
9		0.33	2:1	2.7	64	36	1.8
10	1:3	0.25	3:1	4.1	56	44	1.3
11		0.29	2.4:1	6.3	70	30	2.3
12		0.33	2:1	10.7	59	41	1.4
13	1:5	0.25	3:1	3.8	66	34	1.9
14		0.29	2.4:1	8.3	55	45	1.2
15		0.33	2:1	4.8	62	38	1.6